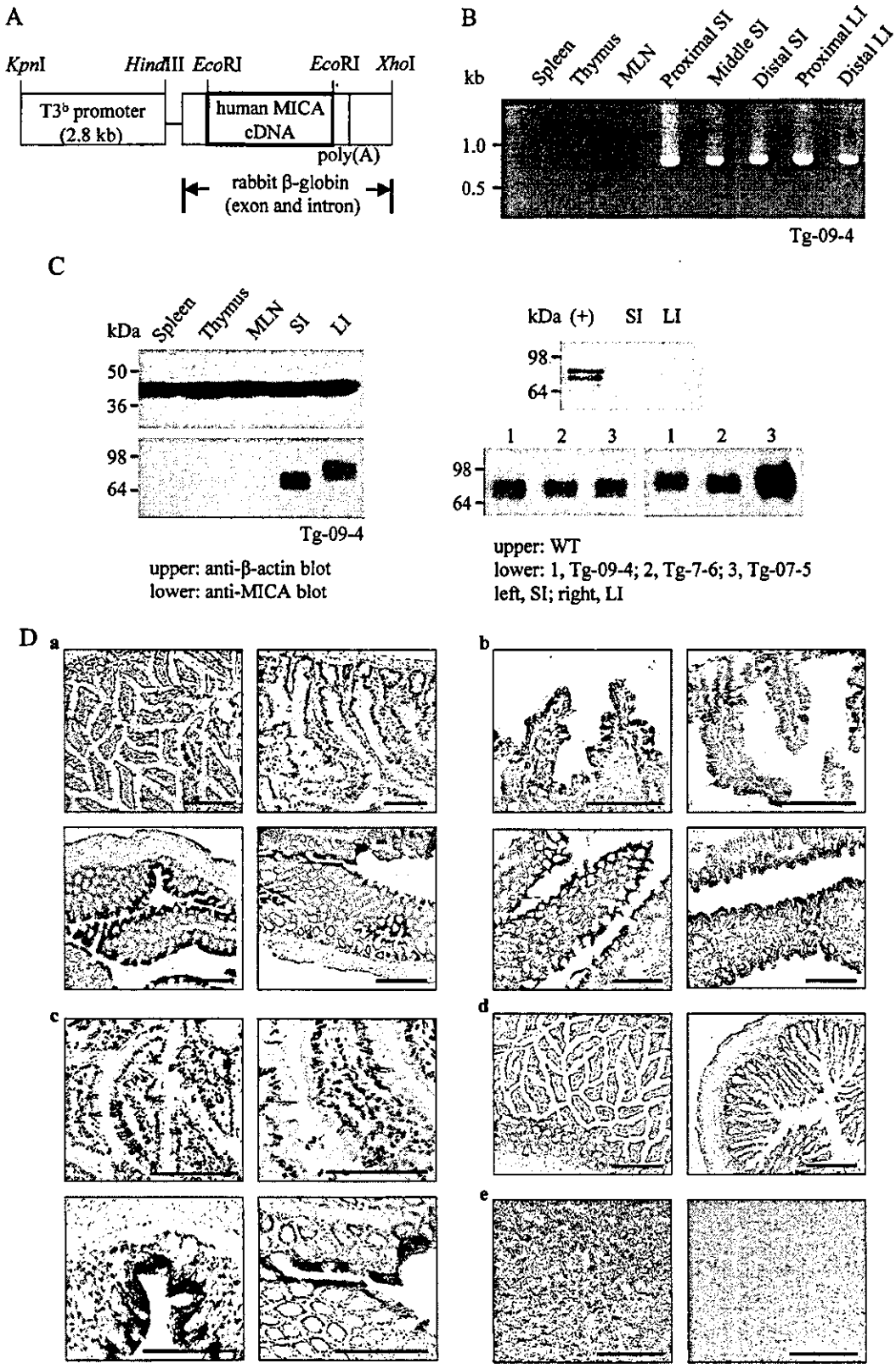

FIGURE 1. Selective expression of MICA in the intestinal tracts of T3^b-MICA Tg mice. *A*, DNA construct. Human MICA cDNA was designed to be expressed in mouse intestinal tracts under the control of the T3^b promoter. *B*, RT-PCR. MICA expression in intestinal tissue of the T3^b-MICA Tg mice was determined by standard RT-PCR, as described in *Materials and Methods*. The expected size of MICA-specific cDNA (0.8 kb) was shown in the lanes of small and large intestines. *C*, Immunoblotting. *Left*, Matured MICA proteins were expressed in small (SI) and large intestinal (LI) tissues, but not in spleen, thymus, and mesenteric lymph node of T3^b-MICA Tg mice. As a loading control, β-actin blot was also used in a separate membrane containing the same amount of whole cell lysates as those of MICA blot. *Right*, MICA was specifically expressed only in small and large intestines from all three lines of Tg mice, but not in non-Tg C57BL/6 mice. *D*, Immunohistochemical assay. The analyses by using anti-MICA mAb (6D4) exhibited that MICA resides in villous of the small intestine (SI) and tip and villous regions of the large intestine (LI). *a*, Tg-09-4; *b*, Tg-07-5; *c*, magnified photographs of Tg-09-4 (*upper*, SI; *lower*, LI; *left*, proximal; *right*, distal region). *d*, C57BL/6 (*left*, SI; *right*, LI). *e*, Tg-09-4 (*left*, spleen; *right*, thymus). MICA protein was expressed both in proximal and distal regions, although the differential pattern of transgenic expression showed large intestine and proximal region were slightly more than small intestine and distal region, respectively. Bars indicate 100 μm.

Table I. *Enumeration of cells for each SI-IEL population in T3^b-MICA Tg lines*[a]

Line	Total IEL	TCRγδ	TCRαβ		
			CD4	CD8 (CD8αβ)	CD4CD8αα (DP)
WT (n = 7)	12.3 ± 2.3	4.4 ± 1.5	0.9 ± 0.3	3.9 ± 1.0 (2.0 ± 0.4)	0.4 ± 0.2
Tg-07-5 (n = 5)	15.2 ± 4.5	4.1 ± 1.0	1.3 ± 0.6	2.7 ± 1.4 (2.0 ± 1.3)	3.9 ± 1.3
Tg-07-6 (n = 3)	12.0 ± 4.2	2.2 ± 1.0	1.5 ± 0.6	2.8 ± 1.6 (2.0 ± 1.1)	2.9 ± 0.9
Tg-09-4 (n = 8)	17.5 ± 6.7	5.8 ± 2.5	1.3 ± 0.5	3.4 ± 1.6 (2.2 ± 0.9)	4.0 ± 2.9

[a] The numbers of cells are indicated as × 10^6 ± SD. n, Number of mice tested. The total cells were prepared from the Percoll gradient interface, as described in *Materials and Methods*. The total number of lymphocytes in each population was calculated by multiplying the percentage of each population determined in Fig. 2 by the total number of lymphocytes.

tissues of the T3^b-MICA Tg and wild-type (WT) mice and subjected to MICA-specific semiquantitative RT-PCR analysis (Fig. 1*B*). Transgenic MICA mRNA was expressed selectively in the gastrointestinal tract, i.e., small and large intestine, but not in other tissues, i.e., spleen, thymus, and mesenteric lymph node, and in none of the same tissues of WT mice. MICA production by intestinal epithelial cells was confirmed also at the protein level by immunoblotting analysis (Fig. 1*C*); by use of anti-MICA mAb 2C10, MICA protein was found in the small and large intestines of T3^b-MICA Tg, but not in those tissues of WT mice. In situ expression of MICA protein was documented also by immunohistological analysis using anti-MICA mAb 6D4; in both the small and large intestine, MICA protein was located in the epithelium, but not in the lamina propria (Fig. 1*D*). MICA was present on most of the villi of the small intestine, and in the colonic epithelium it was concentrated in tip regions; this expression pattern was almost identical in all the lines of Tg mice examined. These combined results established that the human MICA was specifically expressed in the intestinal tracts of the T3^b-MICA Tg mice.

Increase in TCRαβ CD4CD8αα (DP) IELs in the small intestine

IELs from the WT mice and three Tg lines were isolated and analyzed for possible alterations induced by MICA expression in the intestinal epithelium. In the presence of the MICA, the total number of IEL and the numbers of γδ T cells and the CD4 and CD8αβ subsets were not changed (Table I). However, the absolute number as well as the percentage of TCRαβ CD4CD8αα (DP) IELs in the total IEL population were increased 7–10 times, whereas the number of TCRαβ CD8αα IELs was decreased by about one-half (Table I and Fig. 2*A*).

Because MICA expression affected the TCRαβ fraction of IEL, we next compared the changes in these cells between the small and large intestine of the T3^b-MICA Tg mice. In Fig. 2*B*, representative flow cytometry analysis of the TCR Vβ-gated IEL populations in the small intestines of WT mice and the Tg line (Tg-07-6) is illustrated; the population of DP IEL was markedly increased in all the Tg animals examined. In contrast, despite strong expression of MICA in the epithelium of the large intestine, no change in the colonic IEL population was seen (Fig. 2*C*). Splenic cells isolated from the Tg line had the same distribution of CD4 and CD8 T cell populations as that of WT mice (Fig. 2*D*). Thus, locally expressed MICA resulted in increased numbers of TCRαβ CD4CD8αα (DP) IELs selectively in the small intestine.

Maturity of the DP IELs by expression of other surface markers

DP IELs have been proposed to have a distinct origin and to use unique maturation pathways, unlike their thymus counterpart

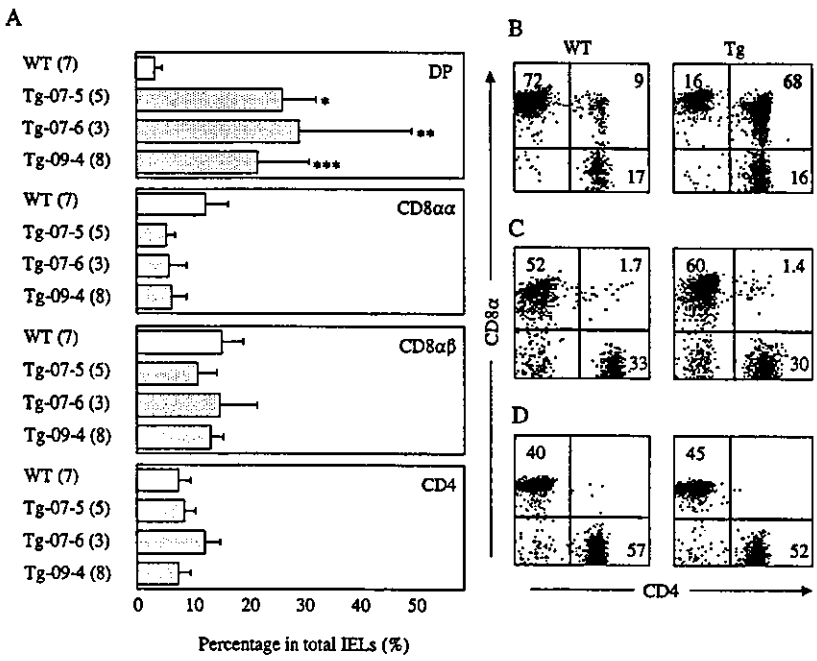

FIGURE 2. Analysis of TCRαβ IEL subsets in WT mice and T3^b-MICA Tg lines. IELs were stained with FITC anti-CD4 or anti-CD8β, PE anti-TCRβ, and APC anti-CD8α mAbs. All the subsets were determined after gating on TCRβ$^+$ cells. The percentage of CD8αα IELs was calculated by subtracting the percentage of TCRαβ CD4CD8αα (DP) IELs from the percentage of TCRαβ CD8αα obtained in the CD8α vs CD8β staining. Statistical comparisons were conducted using Student's two-tailed t test. *, p = 0.0000116; **, p = 0.01183; ***, p = 0.000513 when Tg lines are compared with WT mice. Indicated are results from small intestinal (*B*), large intestinal IEL (*C*), and splenocyte (*D*) of a representative line (Tg-07-6). TCRαβ CD4CD8αα DP IELs in the small intestine were increased (~70% of TCRαβ IELs) compared with those of WT mice (5–10% of TCRαβ IELs) (*B*). The frequency of DP IELs in the large intestine was not augmented in any Tg lines determined (*C*). The frequencies of CD4 and CD8 T cells in spleens of WT and Tg mice were not changed (*D*).

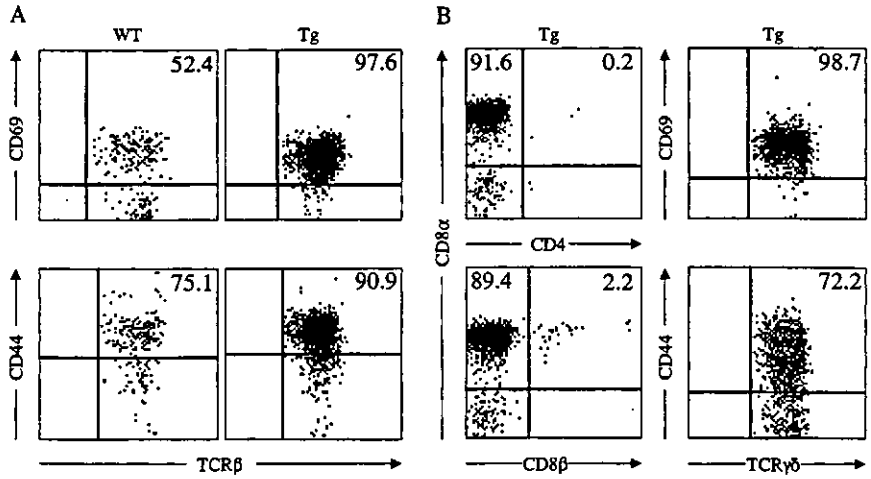

FIGURE 3. Flow cytometric analysis of the DP IELs and γδ IELs of Tg mice for other surface molecules such as maturation markers. *A*, CD4CD8α (DP)-gated population of the Tg mice (*right*) exclusively expressed maturation surface markers CD69 and CD44 in comparison with that of C57BL/6 mice (*left*). *B*, TCRγδ-gated population of the Tg mice mainly expressed CD8αα (*left*) and CD69 and CD44 (*right*), showing the same pattern as that of C57BL/6 mice (data not shown).

(CD8β positive), which expresses low TCR levels and mediates the maturation of CD4 or CD8 T cells (26, 27). When the selectively propagated DP IELs in the T3^b-MICA Tg mice were analyzed for the expression of other surface markers, the cells were shown to exclusively express CD69 and CD44, but not CD62L (data not shown) like those of normal C57BL/6 mice (Fig. 3*A*). When we analyzed the NKG2D expression in DP IELs isolated from Tg and C57BL/6 mice by RT-PCR, the expressions were detected in DP IELs from both mice, even though the expression levels were lower than those of CD8αα IELs (data not shown).

In contrast, there was no change in γδ IEL repertoire in the Tg mice when compared with normal C57BL/6 mice in terms of usage of TCR Vγ and TCR Vδ mRNA, as shown by RT-PCR analysis (data not shown). Moreover, when the phenotype of γδ IELs was examined with respect to CD4, CD8α, and CD8β, the cells prominently expressed CD8αα homodimers, but not CD4 or CD8αβ subsets. The γδ IELs also expressed a high level of CD69 and CD44 (Fig. 3*B*). Thus, the pattern of cell surface markers indicates that the DP IEL and γδ IEL subpopulations have a characteristic of activated T cells (28) and, especially, that the propagated DP IELs are fully mature.

Expansion of the DP IELs expressing Vβ8.1, 8.2 repertoire

To further investigate the nature of the expanded DP IELs, we next characterized the cells' usage of Vβ chains. The total numbers of small intestinal IELs from WT and Tg mice (Tg-09-4 line) used for the Vβ usage analysis were $1.6 \times 10^7 \pm 0.4 \times 10^7$ ($n = 4$, on average) and $1.9 \times 10^7 \pm 0.7 \times 10^7$ ($n = 3$, on average), respectively. The numbers of CD4 and DP IEL were $0.98 \times 10^6 \pm$

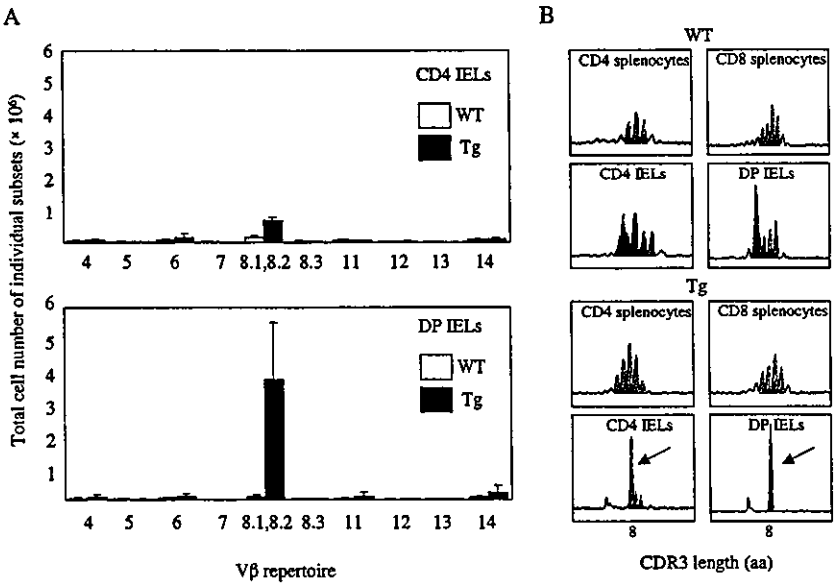

FIGURE 4. *A*, Comparison of the frequency of different Vβ chains expressed by DP T cells in SI-IEL of T3^b-MICA Tg mice. Three WT mice and four mice of the Tg-09-4 line were explored in this flow cytometry analysis. IELs were stained with FITC anti-Vβx, PE anti-CD4, and APC CD8α mAbs. All the subsets were determined after gating on CD4 or CD4 plus CD8α IELs. The total number of lymphocytes in each population was calculated by multiplying the respective percentage of each population. The number of each subset or each Vβ repertoire was calculated by multiplying the respective percentage of each repertoire by the total number of each subset. When splenocytes isolated from the mouse showing the greatest increase in DP IELs (4917×10^6) among four Tg mice were also analyzed by the same method, no significant differences were found between WT and Tg mice (data not shown). *B*, Immunoscope analysis of Vβ8.2 clonotype of CD4 or CD8 T cells from splenocytes and CD4 or DP T cells from SI-IELs of WT or T3^b-MICA Tg mice. Individual populations were purified by cell sorting using FACSVantage. cDNA from each FACS-sorted subset was subjected to PCR using Vβ8.2- and Cβ-specific primers, followed by a runoff with a nested fluorescent Cβ-specific primer (23). The CDR3 size distribution was analyzed with the GeneScan software program. Arrows indicate expansions discussed in the text. The intensity of fluorescence is presented in arbitrary units as a function of CDR3 length in amino acids. The results shown are representative of five individual mice of T3^b-MICA Tg (Tg-09-4 line) and WT mice.

0.32×10^6 and $0.62 \times 10^6 \pm 0.2 \times 10^6$ in WT mice, and $1.64 \times 10^6 \pm 0.64 \times 10^6$ and $5.13 \times 10^6 \pm 1.85 \times 10^6$ in T3^b-MICA Tg mice. As illustrated in Fig. 4*A*, changes were detected in the numbers of CD4 and, especially, DP IELs in the small intestine of T3^b-MICA Tg mice compared with those of WT mice; DP IELs harboring TCR Vβ8.1, 8.2 were markedly expanded ($3.74 \times 10^6 \pm 1.77 \times 10^6$, Tg mice; $0.78 \times 10^5 \pm 0.73 \times 10^5$, WT mice). The increased DP subset compared with that from WT mice was accounted for by this propagated repertoire. We also compared the CD4 and CD8 subsets for Vβ repertoire usage in splenic cells from the Tg mouse line (Tg-07-6) that had the most plentiful DP IELs with these subsets in WT mice. In the absence of MICA, no propagation of the unique T cell clone having the Vβ8.1, 8.2 chain was observed in the splenocytes of the T3^b-MICA Tg mice (data not shown). These results are additional evidence that MICA mediated the clonal expansion of DP IELs expressing the TCR Vβ8.1, 8.2 repertoire in a small intestine-restricted manner.

Clonality of DP IELs expressing TCR Vβ8.2

Using immunoscope analysis associated with DNA sequencing of the CDR3, we next determined the clonality or redundancy of the TCR Vβ8.1, 8.2 chain repertoire used by the DP IELs. By Vβ chain-specific semiquantitative RT-PCR, we found that the expanded repertoire of DP IEL was preferentially associated with the Vβ8.2 chain (data not shown). As shown in Fig. 4*B*, a typical Gaussian distribution of CDR3 lengths of Vβ8.2-Cβ PCR products was observed in the CD4 and CD8 splenocytes from both the WT and Tg mice. The CD4 IEL of the Tg mice had some oligoclonality for the Vβ8.2 chain, compared with that of WT mice (Fig. 4*A*). The DP IEL of interest exhibited a bias of a single peak of CDR3 length for the Vβ8.2 chain in the Tg line, but not in WT mice (Fig. 3*B*). This skewing suggested a clonal expansion of the Vβ8.2-restricted DP IEL induced by MICA. We next analyzed the DNA sequence of the CDR3 region for each amplified Vβ-Jβ combination. As shown in Table II, the Vβ-Jβ pair had a tendency toward the Vβ8.2-Jβ2.7 or Vβ8.2-Jβ1.6 combinations, although this trend was not observed in all the Tg mice. Among the other T3^b-MICA Tg mice examined, Tg-07-5-b mouse showed a Vβ8.2-Jβ2.7 combination containing a major CDR3 sequence (GDPDWEEQ) (8/11), and Tg-07-5-c showed a Vβ8.2-Jβ2.4 combination containing a major CDR3 sequence (SDWGGGQNTL) (6/8). Also, Tg-07-5-d, Tg-07-6-a, and Tg-09-4-d showed a Vβ8.2-Jβ2.5 (GEGLG GKDTQ) (4/5), a Vβ8.2-Jβ1.6 (GPGGRNSPL) (4/6), and a Vβ8.2-Jβ2.1 (SDWGNYAEQ) (4/5), respectively (data not shown). Furthermore, restricted motifs for the CDR3 region in the Vβ8.2-Jβ2.7 and Vβ8.2-Jβ1.6 combination were found to possess a sequence GDRQGFEQ in individual mice in two different lines (Tg-09-4-a and Tg-07-5-a) and SDRGHNSPL in two mice of Tg-09-4 (-b and -c), respectively, whereas no public CDR3 motif for Vβ8.2 chain was detected in the DP among various WT mice. These data imply that MICA-induced clonal expansion of Vβ8.2-harboring DP IEL developed a tendency to restrict limited sequences in the CDR3 region.

Effect of MICA transgene against DSS-induced colitis

It was important to examine physiological and immunological contribution of transgenic MICA in vivo. The T3^b-MICA Tg mice were subjected to the experimental disease-inducing protocol of DSS colitis. The onset of colitis in DSS-treated MICA Tg mice was substantially delayed when compared with that of DSS-treated non-Tg C57BL/6 mice. The DSS-treated MICA Tg mice lost significantly less body weight during the period of the observation

Table II. *Vβ8.2-CDR3 sequence-Jβ chain combination of CD4 and DP subset in SI-IELs*[a]

		CDR3 Sequences for Vβ8.2 Chain		
CD4	WT-a	GAQOTEV-Jβ1.1 (1/8) GDESSPL-Jβ1.6 (1/8) GEPQGTGQL-Jβ2.2 (1/8) GVGRFAATL-Jβ2.3 (1/8) GALGDTL-Jβ2.4 (1/8) GDAAGGRQNTL-Jβ2.4 (1/8) GDWGNNQDTQ-Jβ2.5 (1/8) GGGWPSSYEQ-Jβ2.7 (1/8)	Tg-07-5-a	SDFGNYAEQ-Jβ2.1 (2/12) GDGPGGAETL-Jβ2.3 (1/12) GLGGRAETL-Jβ2.3 (1/12) QGRVQQTQ-Jβ2.3 (1/12) GAGLGDTQ-Jβ2.5 (1/12) GEGRQDTQ-Jβ2.5 (1/12) GDAGYEQ-Jβ2.7 (1/12) GEGLGGREQ-Jβ2.7 (1/12) **GDRQGFEQ-Jβ2.7 (3/12)**
			Tg-07-5-a	Tg-09-4-a
DP	WT-a	SDAAGKAP-Jβ1.5 (3/14) GDRDRGTTGQL-Jβ2.2 (1/14) GAPGQGGQNTL-Jβ2.4 (1/14) GEGLGGRNTL-Jβ2.4 (1/14) GDATGGALDTQ-Jβ2.5 (1/14) GGDWGGATG-Jβ2.5 (4/14) GDAGTYFQ-Jβ2.7 (1/14) GDAQNYEQ-Jβ2.3 (1/14) GDVGDSYEQ-Jβ2.7(1/14)	GEGGGNTL-Jβ2.4 (1/10) **GDRQGFEQ-Jβ2.7 (9/10)**	GARRNQDTQ-Jβ2.5 (1/17) **GDRQGFEQ-Jβ2.7 (16/17)**
			Tg-07-5-b	Tg-09-4-b
			GDPDWEEQ-Jβ2.7 (8/11) GDAGGLSYEQ-Jβ2.7(1/11) GASGEGGGNTL-Jβ2.7 (1/11) GASVWTGLLNQ-J102/2.7 (1/11)	**SDRGHNSPL-Jβ1.6 (6/8)** GDGGLGUAEQ-Jβ2.1 (2/8)
	WT-b	GDRDRGTTGQL-Jβ2.2 (1/6) GEGQGTTGQI-Jβ2.2 (1/6) GGDAQNYEQ-Jβ2.7 (1/6) GDRYEQ-Jβ2.7 (1/6)	Tg-07-5-c	Tg-09-4-c
			GALTTSAETL-Jβ2.3 (1/8) SDWGGGQNTL-Jβ2.4 (6/8) GFGLGGRDTQ-Jβ2.5 (1/8)	**SDRGHNSPL-Jβ1.6 (2/8)** GDWGGGSQNTL-Jβ2.4(2/8) GVGLGGLDT-Jβ2.5 (4/8)

[a] The predominant or expanded sequences are indicated (bold letters). The detection frequencies are determined by the number of sequences with the listed CDR3 sequence of the total number of sequences generated for the particular Vβ8.2-Jβ combination in the mouse indicated.

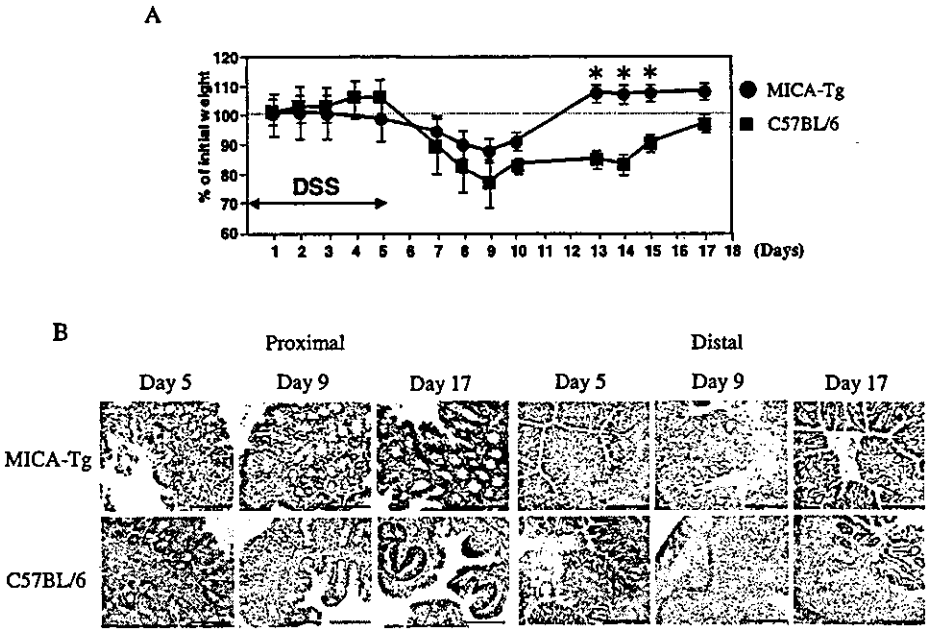

FIGURE 5. The suppressive effect of transgenic MICA for the development of DSS-induced colitis. *A*, Body weight was measured daily. Data shown represent the mean ± SD of mice in each group ($n = 5$) (*, $p < 0.05$). *B*, Histological analysis of colons in DSS-treated MICA Tg mice. The severity of the colitis was also determined in each group of mice ($n = 3$) by using the histological disease-scoring system (25). The transgenic MICA ameliorated the severity of the colitis. Bars indicate 50 μm (proximal colon) and 100 μm (distal colon).

when compared with DSS-treated non-Tg mice (Fig. 5*A*). The frequency of the physical change typical of those in DSS-treated C57BL/6 mice, i.e., hunched posture, anorectal prolapse, and diarrhea, was less observed in the DSS-treated MICA Tg mice. Histological analysis of colons, especially distal portion, from the DSS-treated MICA Tg mice revealed that the occurrence of ulcer, abscess, diminution of goblet cells, and disturbance of tissue architecture by infiltration of inflammatory neutrophils and mononuclear cells were reduced in the DSS-treated MICA Tg mice compared with DSS-treated C57BL/6 mice (Fig. 5*B*). Furthermore, recovery of the regeneration of epithelial layer and damaged tissue architecture was more rapidly observed in the DSS-treated MICA Tg mice compared with DSS-treated C57BL/6 mice. The average score in DSS-treated MICA Tg mice (e.g., proximal and distal colon; 4 and 1 on day 17, respectively) was less than that in DSS-treated C57BL/6 mice (proximal and distal colon; 8 and 12 on day 17, respectively). Thus, although MICA Tg mice developed mild acute-type colitis by administration of DSS, the severity of the colitis was markedly diminished compared with non-Tg mice.

Discussion

In this study, we report the generation of a Tg model expressing human MICA selectively in mouse intestine. The $T3^b$-MICA Tg mice possess some interesting properties. First, the mice expressed the MICA only in the intestinal tract (small intestinal villi and large intestinal tips). Second, the mice contained a greatly increased CD4CD8$\alpha\alpha$ (DP) IEL in the small, but not the large intestine, and this population was present only in the IEL, not in lamina propria lymphocyte. Third, the increased DP subset was almost entirely biased toward the Vβ8.2 chain repertoire, with some restricted CDR3 sequences. Based on these results, it is evident that the overexpression of intestinal MICA specifically promoted the development of clonally expanded DP IELs in the small intestine.

A major reason we chose to express intestinal MICA by the use of the $T3^b$ promoter was that both the $T3^b$ (a thymic leukemia Ag) and the MICA are nonclassical MHC class Ib molecules, and it has been reported that both of them are preferentially expressed in the intestinal epithelial cells (14, 19, 29). Thus, it could be expected that the $T3^b$-driven MICA molecule expressed in the murine intestinal immune system would be represented and behave physiologically in the in vivo situation. In addition, our recent separate results showed that transgenic MICA is preferentially expressed in the basolateral side of the intestinal epithelial cells (data not shown), as previously reported (30). Thus, MICA and its derived mucosal T cells may be important components of the innate regulatory network that maintains immunologic homeostasis in the harsh environment of the intestinal tract. In this regard, $T3^b$ promoter-driven, transgenic MICA was able to attenuate the DSS-induced intestinal inflammation (Fig. 5), indicating the basolateral expression of MICA in intestinal epithelia be appropriate for the immunological surveillance against mucosal inflammation.

CD4CD8$\alpha\alpha$ (DP) lymphocytes in mice are present mainly in the small intestine and, unlike thymic DP T cells, highly express CD3 on their surfaces (31). This interesting subset, harboring mutually exclusive coreceptors, is proposed to be involved in intestinal T cell maturation and development, and possibly to function in both innate and adaptive immunity (32). DP IELs have been shown capable of secreting Th2-type cytokines and providing help to B cells for the secretion of Igs (33). Also, TCR$\alpha\beta$-mediated signaling initiated cytotoxic function, but did not induce proliferation of the DP IELs (34), and murine CD4 IELs were found to give rise to DP IELs in an inflammatory bowel disease model (35). Recently, it was shown that $CD4^+CD8\alpha\alpha$ T cells in the intestinal epithelium were functioning as regulatory T cells for the prevention of inflammatory bowel disease in an IL-10-dependent fashion (36). Together with this report (37) and our present finding that $T3^b$-MICA Tg mice are resistant to the development of DSS-induced colitis, an interesting scenario would be that a stress-associated nonclassical MHC class I molecule participates in the preferential induction of DP IELs with a regulatory function for the maintenance of host immune homeostasis from the development of the intestinal inflammation. Although the ontogeny, function, and precise reason for the propagation of DP IELs remain to be clarified, our unique $T3^b$-MICA Tg mouse model most likely will be useful for this purpose.

There is evidence that DP IELs arise from thymus-derived CD4 T cells, which migrate into the epithelium and express CD8 (32); a report that the transfer of CD4 peripheral T cells into SCID mice

reconstituted DP IELs also supports this view (35). Furthermore, both CD4 and DP subsets of rat IELs reportedly showed oligoclonality and overlapping β-chain repertoires, and the DP subset contains a considerably more restricted repertoire than do $CD4^+$ IELs (37). Our data from immunoscope and CDR3 sequence analyses also reveal that DP IELs have more restricted oligoclonality than do CD4 IELs in $T3^b$-MICA Tg mice (Fig. 3 and Table II). However, in addition to the possibility that DP IELs mature from CD4 IELs, it is possible that $CD8\alpha\alpha$ IELs transform into DP IELs by acquisition of the CD4 coreceptor under the influence of MICA in the intestinal epithelium. As depicted in Fig. 2A, contrary to $TCR\alpha\beta$ CD4 or $CD8\alpha\beta$ population exhibiting no quantitative alteration, the percentage of $CD8\alpha\alpha$ IELs was no more than 50% of those in WT mice, while $CD4CD8\alpha\alpha$ (DP) IELs were concurrently increased in all Tg lines; perhaps this result reflects maturation of $CD8\alpha\alpha$ IELs into $CD4CD8\alpha\alpha$ IELs.

An intriguing question is what is the driving force responsible for human MICA accelerating a bias to clonal selection of DP IELs and their propagation? Some interesting possibilities can be entertained. First, the transgenic MICA molecules could be recognized by an NKG2D-like or -related receptor for MICA, expressed on the DP IELs. In this regard, in a separate study, we are assessing the reactivity of the NKG2D tetramer with intestinal epithelial cells (IECs) isolated from the small intestine of the $T3^b$- MICA Tg mice by flow cytometric analysis and immunohistochemical analysis. We have found that IECs isolated from the MICA Tg, but not WT, mice bind strongly to the NKG2D tetramer, and an intense signal is present in the basolateral portions of IECs (data not shown). In contrast, splenocytes isolated from both $T3^b$- MICA Tg and WT mice did not react with the NKG2D tetramer. These results suggest that ectopically expressed MICA molecules in the Tg mice can interact specifically with NKG2D molecules on neighboring IELs in a physicochemical fashion. Second, $CD8\alpha\alpha$ coreceptors on DP IEL could directly bind to MICA independent of TCR specificity, similar to the reported interaction between $CD8\alpha\alpha$ and the thymic leukemia Ag, which is another nonclassical MHC class I molecule expressed on intestinal epithelial cells, modulating T cell responses (38). And the lack of expansion of γδ IELs in the small intestine of the $T3^b$-MICA Tg mice might be due to the species (rodents vs humans), aging (adults vs neonates), and/or tissue (small vs large intestine) differences. In this regard, our unpublished data demonstrated that MICA could positively regulate the development of γδ IELs in the neonatal stage of the $T3^b$-driven MICA Tg mice and in the early phase of bone marrow-chimeric irradiated MICA-Tg/RAG-2-deficient mice.

In our Tg mice, MICA was designed to be expressed in both the small and large intestine, and indeed both sites harbored many MICA proteins. However, the prominent change in IELs was only restricted to the small intestine. One possible explanation for this observation might be differences in the commensal microflora. In the colon, the symbiotic microbes might block the ability of MICA to increase DP IELs by protecting the colonic epithelium and intraepithelial T cells from stress-induced inflammation. Alternatively, the different effects on IELs might reflect qualitative and quantitative differences in the IEL subsets residing in the small and large intestines; large intestinal IELs contain more CD4 T cells with a lower frequency of DP T cells than do small intestinal IELs (39, 40). Collectively, we emphasize that our $T3^b$-MICA Tg mice are a unique in vivo model that can be used to elucidate the biological role of the stress-inducible nonclassical MHC molecules for the regulation of gastrointestinal immune surveillance and homeostasis.

Acknowledgments

We thank Dr. Toshiro Suzuki at Japan SLC for his help in generating $T3^b$-MICA Tg mice, Dr. Olga Naidenko (Washington University, St. Louis, MO) for kind provision with NKG2D tetramer, Dr. Masami Nozaki at Central Instrumentation Laboratory of The Research Institute for Microbial Diseases in Osaka University for his help in DNA sequence analysis, and Dr. William Brown (University of Colorado School of Medicine, Denver, CO) for his critical reading of the manuscript.

References

1. Matsuzaki, G., T. Lin, and K. Nomoto. 1994. Differentiation and function of intestinal intraepithelial lymphocytes. *Int. Rev. Immunol. 11:47.*
2. Beagley, K., and A. Husband. 1998. Intraepithelial lymphocytes: origins, distribution, and function. *Crit. Rev. Immunol. 18:237.*
3. Hayday, A., E. Theodoridis, E. Ramsburg, and J. Shires. 2001. Intraepithelial lymphocytes: exploring the Third Way in immunology. *Nat. Immun. 2:997.*
4. Poussier, P., and M. Julius. 1994. Thymus independent T cell development and selection in the intestinal epithelium. *Annu. Rev. Immunol. 12:521.*
5. Guy-Grand, D., and P. Vassalli. 2002. Gut intraepithelial lymphocyte development. *Curr. Opin. Immunol. 14:255.*
6. Lin, T., G. Matsuzaki, H. Kenai, and K. Nomoto. 1995. Extrathymic and thymic origin of murine IEL: are most IEL in euthymic mice derived from the thymus?. *Immunol. Cell Biol. 73:469.*
7. Lefrancois, L., and L. Puddington. 1995. Extrathymic intestinal T-cell development: virtual reality?. *Immunol. Today 16:16.*
8. Suzuki, K., T. Oida, H. Hamada, O. Hitotsumatsu, M. Watanabe, T. Hibi, H. Yamamoto, E. Kubota, S. Kaminogawa, and H. Ishikawa. 2000. Gut cyrptopatches: direct evidence of extrathymic anatomical sites for intestinal T lymphopoiesis. *Immunity 13:691.*
9. Leishman, A. J., L. Gapin, M. Capone, E. Palmer, H. R. MacDonald, M. Kronenberg, and H. Cheroutre. 2002. Precursors of functional MHC class I- or II-restricted $CD8\alpha\alpha^+$ T cells are positively selected in the thymus by agonist self-peptides. *Immunity 16:355.*
10. Wurbel, M.-A., M. Malissen, D. Guy-Grand, E. Meffre, M. C. Nussenzweig, M. Richelme, A. Carrier, and B. Malissen. 2001. Mice lacking the CCR9 CC-chemokine receptor show a mild impairment of early T- and B-cell development and a reduction in T-cell receptor $\gamma\delta^+$ gut intraepithelial lymphocytes. *Blood 98:2626.*
11. Bahram, S. 2001. MIC genes: from genetics to biology. *Adv. Immunol. 76:1.*
12. Groh, V., S. Bahram, S. Bauer, A. Herman, M. Beauchamp, and T. Spies. 1996. Cell stress-regulated human major histocompatibility complex class I gene expressed in gastrointestinal epithelium. *Proc. Natl. Acad. Sci. USA 93:12445.*
13. Groh, V., R. Rhinehart, H. Secrist, S. Bauer, K. H. Grabstein, and T. Spies. 1999. Broad tumor-associated expression and recognition by tumor-derived γδ T cells of MICA and MICB. *Proc. Natl. Acad. Sci. USA 96:6879.*
14. Groh, V., A. Steinle, S. Bauer, and T. Spies. 1998. Recognition of stress-induced MHC molecules by intestinal epithelial γδ T cells. *Science 279:1737.*
15. Bauer, S., V. Groh, J. Wu, A. Steinle, J. H. Phillips, L. L. Lanier, and T. Spies. 1999. Activation of NK cells and T cells by NKG2D, a receptor for stress-inducible MICA. *Science 285:727.*
16. Das, H., V. Groh, C. Kuijl, M. Sugita, C. T. Morita, T. Spies, and J. F. Bukowski. 2001. MICA engagement by human $V\gamma2V\delta2$ T cells enhances their antigen-dependent effector function. *Immunity 15:83.*
17. Pardoll, D. M. 2001. Stress, NK receptors and immune surveillance. *Science 294:534.*
18. Kronenberg, M., and H. Cheroutre. 2000. Do mucosal T cells prevent intestinal inflammation? *Gastroenterology 118:974.*
19. Aihara, H., N. Hiwatashi, S. Kumagai, Y. Obata, T. Shimosegawa, T. Toyota, and J.-I. Miyazaki. 1999. The T3(b) gene promoter directs intestinal epithelial cell-specific expression in transgenic mice. *FEBS Lett. 463:185.*
20. Ohta, N., T. Hiroi, M.-N. Kweon, N. Kinoshita, M. H. Jang, T. Mashimo, J.-I. Miyazaki, and H. Kiyono. 2002. IL-15-dependent activation-induced cell death-resistant Th1 type $CD8\alpha\beta^+NK1.1^+$ T cells for the development of small intestinal inflammation. *J. Immunol. 169:460.*
21. Groh, V., R. Rhinehart, J. Randolph-Habecker, M. S. Topp, S. R. Riddell, and T. Spies. 2001. Costimulation of $CD8\alpha\beta$ T cells by NKG2D via engagement by MIC induced on virus-infected cells. *Nat. Immun. 2:255.*
22. Yamamoto, M., K. Fujihashi, K. Kawabata, J. R. McGhee, and H. Kiyono. 1998. A mucosal intranet: intestinal epithelial cells down-regulate intraepithelial, but not peripheral, T lymphocytes. *J. Immunol. 160:2188.*
23. Takahashi, I., J. Matsuda, L. Gapin, H. DeWinter, Y. Kai, H. Tamagawa, M. Kronenberg, and H. Kiyono. 2002. Colitis-related public T cells are selected in the colonic lamina propria of IL-10-deficient mice. *Clin. Immunol. 102:237.*
24. Kabashima, K., T. Saji, T. Murata, M. Nagamachi, T. Matsuoka, E. Segi, K. Tsuboi, Y. Sugimoto, T. Kobayashi, Y. Miyachi, et al. 2002. The prostaglandin receptor EP4 suppresses colitis, mucosal damage and CD4 cell activation in the gut. *J. Clin. Invest. 109:883.*
25. DeWinter, H., D. Elewaut, O. Turovskaya, M. Huflejt, C. Shimeld, A. Hagenbaugh, S. Binder, I. Takahashi, M. Kronenberg, and H. Cheroutre. 2002. Regulation of mucosal immune responses by recombinant interleukin 10 produced by intestinal epithelial cells in mice. *Gastroenterology 122:1829.*
26. Zuckermann, F. A. 1999. Extrathymic CD4/CD8 double positive T cells. *Vet. Immunol. Immunopathol. 72:55.*

27. Lefrancois, L. 1991. Phenotypic complexity of intraepithelial lymphocytes of the small intestine. *J. Immunol. 147:1746.*
28. Tough, D. F., S. Sun, X. Zhang, and J. Sprent. 1999. Stimulation of naïve and memory T cells by cytokines. *Immunol. Rev. 170:39.*
29. Hershberg, R., P. Eghtesady, B. Sydora, K. Brorson, H. Cheroutre, R. Modlin, and M. Kronenberg. 1990. Expression of the thymus leukemia antigen in mouse intestinal epithelium. *Proc. Natl. Acad. Sci. USA 87:9727.*
30. Suemizu, H., M. Radosavljevic, M. Kimura, S. Sadahiro, S. Yoshimura, S. Bahram, and H. Inoko. 2002. A basolateral sorting motif in the MICA cytoplasmic tail. *Proc. Natl. Acad. Sci. USA 99:2971.*
31. Mosley, R. L., D. Styre, and J. R. Klein. 1990. $CD4^+CD8^+$ murine intestinal intraepithelial lymphocytes. *Int. Immunol. 2:361.*
32. Reimann, J., and A. Rudolphi. 1995. Co-expression of $CD8\alpha$ in $CD4^+$ T cell receptor $\alpha\beta^+$ T cells migrating into the murine small intestine epithelial layer. *Eur. J. Immunol. 25:1580.*
33. Fujihashi, K., M. Yamamoto, J. R. McGhee, and H. Kiyono. 1993. $\alpha\beta$ T cell receptor-positive intraepithelial lymphocytes with $CD4^+$, $CD8^-$ and $CD4^+$, $CD8^+$ phenotypes from orally immunized mice provide Th2-like function for B cell responses. *J. Immunol. 151:6681.*
34. Sasahara, T., H. Tamauchi, N. Ikewaki, and K. Kubota. 1994. Unique properties of a cytotoxic $CD4^+CD8^+$ intraepithelial T-cell line established from the mouse intestinal epithelium. *Microbiol. Immunol. 38:191.*
35. Morrissey, P. J., K. Charrier, D. A. Horovitz, F. A. Fletcher, and J. D. Watson. 1995. Analysis of the intra-epithelial lymphocyte compartment in SCID mice that received co-isogenic $CD4^+$ T cells: evidence that mature post-thymic $CD4^+$ T cells can be induced to express $CD8\alpha$ in vivo. *J. Immunol. 154:2678.*
36. Das, G., M. M. Augustine, J. Das, K. Bottomly, P. Ray, and A. Ray. 2003. An important regulatory role for $CD4^+CD8\alpha\alpha$ T cells in the intestinal epithelial layer in the prevention of inflammatory bowel disease. *Proc. Natl. Acad. Sci. USA 100:5324.*
37. Helgeland, L., F.-E. Johansen, J. O. Utgaard, J. T. Vaage, and P. Brandtzaeg. 1999. Oligoclonality of rat intestinal intraepithelial T lymphocytes: overlapping TCR β-chain repertoires in the CD4 single-positive and CD4/CD8 double-positive subsets. *J. Immunol. 162:2683.*
38. Leishman, A. J., O. V. Naidenko, A. Attinger, F. Koning, C. J. Lena, Y. Xiong, H.-C. Chang, E. Reinherz, M. Kronenberg, and H. Cheroutre. 2001. T cell responses modulated through interaction between $CD8\alpha\alpha$ and the nonclassical MHC class I molecule, TL. *Science 294:1936.*
39. Beagley, K. W., K. Fujihashi, A. S. Lagoo, S. Lagoo-Deenadaylan, C. A. Black, A. M. Murray, A. T. Sharmanov, M. Yamamoto, J. R. McGhee, C. O. Elson, and H. Kiyono. 1995. Differences in intraepithelial lymphocyte T cell subsets isolated from murine small versus large intestine. *J. Immunol. 154:5611.*
40. Camerini, V., C. Panwala, and M. Kronenberg. 1993. Regional specialization of the mucosal immune system: intraepithelial lymphocytes of the large intestine have a different phenotype and function than those of the small intestine. *J. Immunol. 151:1765.*

0023-6837/03/8307-1045$03.00/0
LABORATORY INVESTIGATION

Vol. 83, No. 7, p. 1045, 2003
Printed in U.S.A.

Characteristics of Claudin Expression in Follicle-Associated Epithelium of Peyer's Patches: Preferential Localization of Claudin-4 at the Apex of the Dome Region

Hiroshi Tamagawa, Ichiro Takahashi, Mikio Furuse, Yuka Yoshitake-Kitano, Shoichiro Tsukita, Toshinori Ito, Hikaru Matsuda, and Hiroshi Kiyono

Department of Surgery (HT, TI, HM), Osaka University Graduate School of Medicine, and Department of Mucosal Immunology (HT, IT, HK), Research Institute for Microbial Diseases, Osaka University, Osaka, and Department of Preventive Dentistry & Host Defense (IT), Hiroshima University Graduate School of Biomedical Sciences, Hiroshima, and Department of Cell Biology (MF, YY-K, ST), Faculty of Medicine, Kyoto University Graduate School, Kyoto, Division of Mucosal Immunology (HK), Department of Microbiology and Immunology, The Institute of Medical Science, The University of Tokyo, and CREST, JST (HK), Tokyo, Japan

SUMMARY: Gut-associated lymphoreticular tissues, such as Peyer's patches and cecal patches, are important inductive sites for mucosal immune responses. As such, gut-associated lymphoreticular tissues may have an epithelial barrier different from that of villous epithelium. In this study, we investigated the immunohistochemical distribution of the claudin family and occludin in the follicle-associated epithelium (FAE) of Peyer's patches and cecal patches of murine intestine. Unique profiles of claudin-2, -3, and -4 and occludin expression were noted in the tight junctions of the FAE: claudin-4 was preferentially expressed in the apex region; claudin-2 was only weakly expressed on the crypt side of the FAE compared with stronger expression on the crypt side of villous epithelial cells; and claudin-3 and occludin were found throughout the dome. These unique expression patterns were present also in cecal patch FAE. We also found that claudin-4 expression in the FAE of Peyer's patches and cecal patches correlated with the presence of TUNEL (terminal deoxynucleotidyl transferase-mediated dUTP nick-end labeling)-positive apoptotic cells, and Peyer's patch-deficient mice exhibited expression patterns of claudin and occludin in villous epithelia similar to those in wild-type mice. We conclude that claudin-4 expression was preferentially associated with the dome region of FAE, the mucosal inductive site of the murine intestine. In that location it might correlate with the cell life cycle, help maintain the apex configuration of the dome, or be a factor favoring the uptake of antigens by the FAE. (*Lab Invest 2003, 83:1045–1053*).

The intestinal mucosa is covered with one layer of epithelium. Enterocytes are generated from stem cells in the crypts, become mature forms, and migrate to the tips of the villi. The cells, which are continually renewed, have a life span of 2 to 4 days (Creamer, 1967). To maintain homeostasis and preserve the integrity of the epithelial barrier, the intercellular junctional complex, which consists of tight junctions, adherens junctions, and desmosomes, is thought to facilitate appropriate communication between outside and inside environments. Of these mechanisms, tight junctions located at the most apical side play a central role in sealing the intercellular space on epithelial sheets (Anderson and Van Itallie, 1995; Schneeberger and Lynch, 1992; Tsukita et al, 2001). Several proteins, mainly occludin (Furuse et al, 1993) and claudin (Furuse et al, 1998; Morita et al, 1999a), comprise the tight junctions. Various cells, organs, and parts of tissue have unique distributions of the various claudins. According to a recent report, claudin-2, -3, -4, and -5 are highly expressed in the rat intestine (Rahner et al, 2001).

Peyer's patches (PP) are an important gut-associated lymphoreticular tissue (GALT) and are critical in the priming of antigen-specific T helper 1/T helper 2 cells and IgA-committed B cells, with dissemination of the primed lymphocytes to distant mucosal sites for the generation of antigen-specific IgA immune responses. Like other secondary lymphoid tissues, PP contain all of the necessary lymphoreticular cells, including APCs (macrophages and dendritic cells), lymphocytes, and supporting stromal cells for the induction of antigen-specific humoral and cellular immunity (McGhee and Kiyono, 1999). One of the unique features of this lymphoid tissue is the presence of an epithelium, called follicle-associated epithelium (FAE), which covers the dome of the patches (Owen,

DOI: 10.1097/01.LAB.0000078741.55670.6E

Received February 28, 2003.
Address reprint requests to: Dr. H. Kiyono, Division of Mucosal Immunology, The Institute of Medical Science, The University of Tokyo, 4-6-1 Shirokanedai, Minato-ku, Tokyo, 108-8639 Japan. E-mail: kiyono@ims.u-tokyo.ac.jp

1977; Owen et al, 1991). Furthermore, M cells, one of the major components of the FAE, are key antigen-sampling cells for the delivery of orally encountered antigens to the underlying APCs (Neutra et al, 1996).

Some intestinal bacteria, eg, *Salmonella*, can invade the intestinal tract through M cells (Kohbata et al, 1986; Savidge et al, 1991). Two possible pathways for the uptake of these and other luminal antigens have been suggested: a transcellular pathway and a paracellular pathway (Atisook and Madara, 1991; Kops et al, 1996). Some kinds of *Salmonella* reportedly can invade also through villous epithelial cells (Niedergang et al, 2000; Vazquez-Torres et al, 1999); this invasion may be mediated by submucosal dendritic cells, which possess dendrites that extend toward the intestinal lumen between the epithelial cells (Rescigno et al, 2001). Claudin-1 (and also occludin) seem to be critical for the maintenance of the tight barrier between enterocytes and dendritic cells. In addition to involvement in the formation of tight junctions, the claudin family functions as a receptor for microorganism-derived molecules. For example, *Clostridium perfringens* enterotoxin binds to claudins, especially to the second loop of claudin-3 and -4 (Fujita et al, 2000; Sonoda et al, 1999). These phenomena suggest that bacteria-originated macromolecules can pass through paracellular pathways by modifying tight junctions. Further, it is also possible that the claudin family acts as a signaling receptor for communication between eukaryotic and parakaryotic cells.

This study was aimed at clarifying whether mucosal inductive tissues, such as PP and cecal patches, have tight junction strands in their FAE that differ from those in villous epithelia.

Results

Claudin and Occludin Expression in Murine Villous Epithelium

We first examined immunohistochemically the expression of claudin and occludin in murine intestinal epithelium. As expected from previous studies in rat intestine (Rahner et al, 2001), occludin was expressed throughout the mucosa of the small intestine (jejunum, Fig. 1A) and large intestine (cecum, Fig. 1B; rectum, data not shown). Among claudin family members, claudin-2 was expressed only in the gland crypts of small and large intestines, whereas claudin-3 was expressed in both the villi and the crypts. Claudin-4 was expressed sparsely in villous tips in the small and large intestines. Occludin, like claudin-3, was present on villi and crypts. Although claudin-2, -3, and occludin seemed to be localized preferentially on the apical side of the epithelial cells, claudin-4 was expressed stronger on the basolateral sides rather than on the apical sides. The different location of claudin staining pattern was clearly shown when the sections were costained with claudin family and ZO-1, a well-known tight junction marker (Fig. 1C). Although the expression of claudin-2, -3, and occludin were common in any parts of intestinal epithelia, our findings clearly indicate the expression of claudin-4 by selective sites, not at every tip of villous epithelium.

Unique Characteristics of Claudin and Occludin Expression in FAE of PP and Cecal Patch

We next examined the expression of claudins and occludin in the FAE of PP (Fig. 2, A and B). Occludin and claudin-3 seemed to be expressed on the FAE and on the villous epithelium, from the crypt side of the FAE to the tip of the dome. Claudin-2 was faintly expressed in a restricted region near the crypt bases where claudin-2 was well expressed in case of villous epithelium. In contrast, claudin-4 was preferentially expressed in the FAE dome, and its expression was stronger than in villous tips. We also examined the distribution of claudins and occludin in the FAE of lymphoid patches present in the cecal wall (Fig. 2C). The expression patterns of these proteins were similar to those in PP: claudin-3 and occludin were expressed throughout the FAE, whereas claudin-2 was only faintly expressed at crypt bases, and claudin-4 was prominently expressed at the tops of the dome. In comparison to PP, cecal patches had large aggregates with overlying broad areas of epithelium, and claudin-4 was correspondingly extensively expressed.

Moreover, claudin-4 in the FAE was localized not only on the apical side but also on the basolateral side of epithelial cells (Fig. 2D), whereas in the villous tip it was exclusively expressed in the basolateral side. Costaining with ZO-1– and claudin-4–specific antibodies made the differences more distinguishable. ZO-1 was expressed only in the apical side of the epithelial cell through the dome of the PP. On the other hand, claudin-4 was found on the apical side as linear signal and vaguely on the basolateral side of the epithelial cells (Fig. 2D). Moreover the expression pattern of claudin-4 on the basal side of FAE was quite different from villous epithelia. These findings further illustrate that claudin-4 expression in FAE of PP was distinctively different from that of intestinal villous epithelium.

Claudin-4–Specific mRNA Expression by the FAE of PP

To confirm the immunohistochemical finding for the preferential expression of claudin-4 on the FAE dome (Fig. 2), we further examined the expression level of claudin-4– specific mRNA in epithelial cells isolated from PP and different locations of villous epithelium (Fig. 3). Thus, epithelial cells were isolated from the FAE dome and two distinct sites (tip and crypt regions) of jejunum. Total RNA was isolated from FAE (*lane 1*) and crypt (*lane 2*) and tip (*lane 3*) portions of villous epithelium for the semiquantative RT-PCR analysis (Fig. 3). The level of occludin mRNA expression was similar among different specimens. However, the level of claudin-4 expression was strong in epithelial cells isolated from FAE of PP and the tip of villous epithelium when compared with the crypt of villous epithelium. These RT-PCR data also supported our immunohistochemical findings in which claudin-4

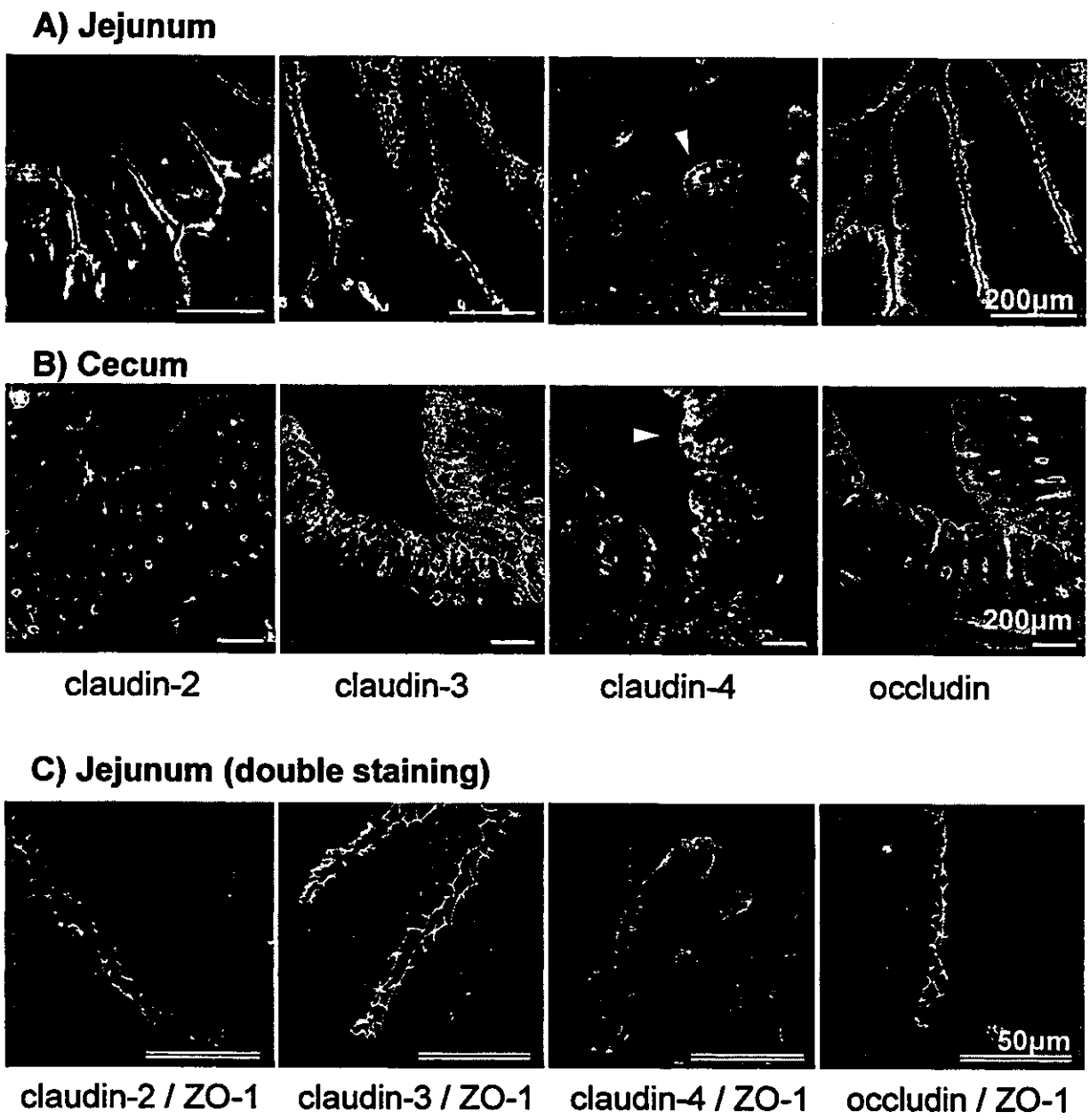

Figure 1.

Claudin and occludin expression in villous epithelia of murine jejunum and cecum. Immunohistochemical staining of claudin-2, -3, -4, and occludin in murine jejunum (A), cecum (B), and costaining with individual claudin (FITC) and ZO-1 (Cy-3) in jejunum (C). Specimens were cryosectioned (6 μm) and stained with primary polyclonal antibodies specific for the respective claudin as well as occludin and ZO-1–specific mAbs, followed by secondary antibodies conjugated with FITC or Cy-3. Claudin-2 is expressed in the crypt region of jejunum and cecum, whereas claudin-3 is expressed in both crypts and villi. Claudin-4 is present sparsely on villous tip cells in the small and large intestines. Occludin, like claudin-3, is expressed by both crypt cells and villous cells. C, Claudin-2, claudin-3, and occludin are expressed on the apical side of the epithelium, but claudin-4 is expressed on the basolateral sides and on the apical sides of epithelial cells. Yellow *arrowheads* indicate examples of claudin-4–positive epithelial cells.

expression was associated with the FAE dome of PP and the tip of villous epithelium.

Possible Association Between Claudin-4 Expression and Apoptosis of Epithelial Cells and FAE of GALT

The localization of claudin-4 in villous tip epithelium and the dome FAE of PP and cecal patches reminded us of the distribution of apoptotic cells in these tissues. Thus, we performed TUNEL (terminal deoxynucleotidyl transferase-mediated dUTP nick-end labeling) staining for the detection of apoptotic cells in the villous epithelium and GALT. Jejunal epithelium had a few TUNEL-positive cells at the apices of villi (Fig. 4A). TUNEL-positive cells were more frequently found in the FAE of PP and cecal patches. Thus, the distribution of TUNEL-positive cells was well correlated with that of claudin-4 in these sites (Fig. 4B).

To further confirm this immuohistochemical observation, a quantitative analysis for the evaluation of

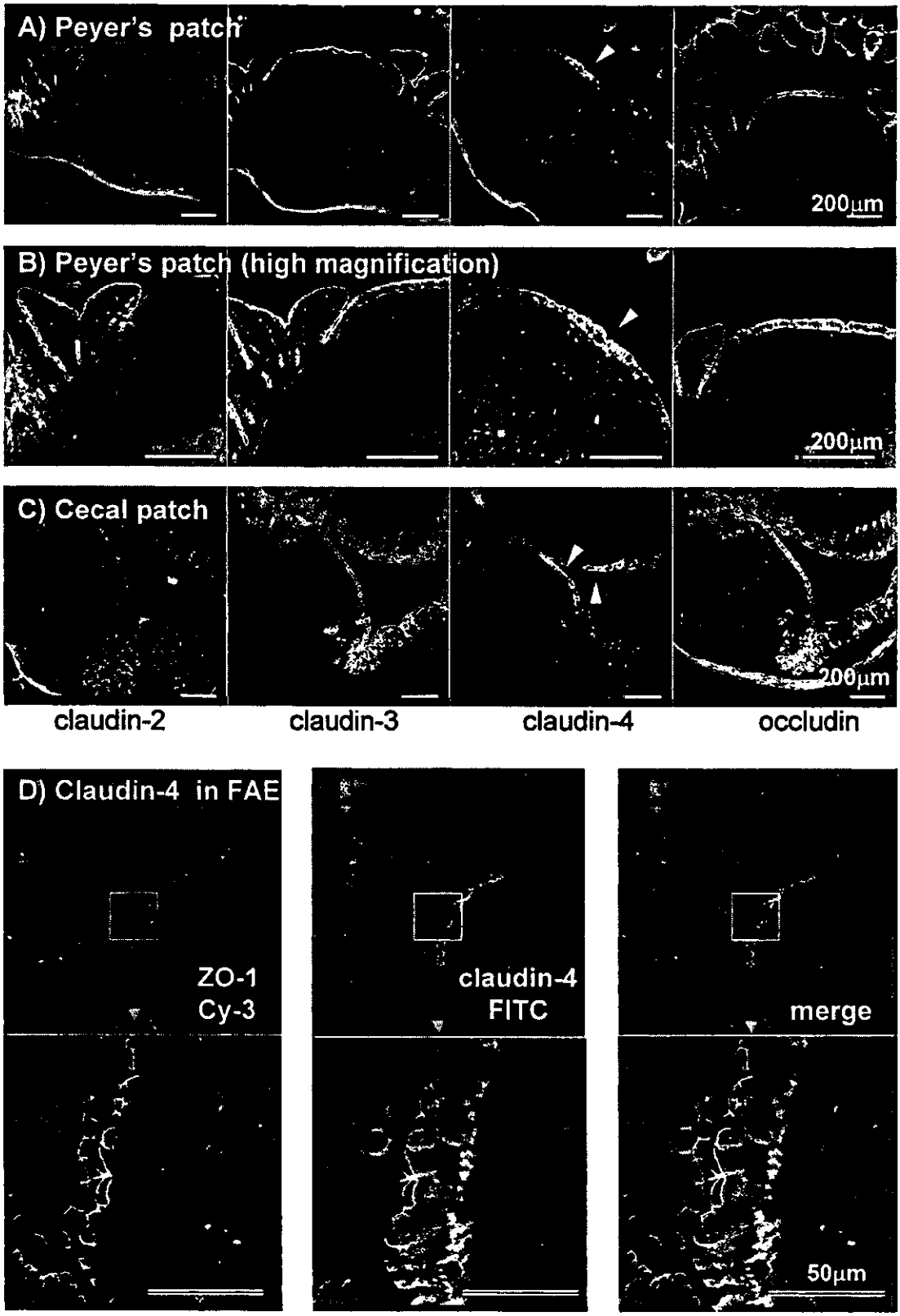

Figure 2.

Claudin expression in Peyer's patches (PP) and cecal patches. Immunohistochemical staining of claudin-2, -3, -4, and occludin in murine PP in jejunum (A; low magnification, B; high magnification) and cecal patched (C). A and B, Claudin-2 is just faintly expressed in the restricted region near the crypt. Claudin-3 and occludin are expressed through the follicle-associated epithelium (FAE). Claudin-4 is preferentially expressed in the tip of the FAE dome compared with villous epithelium. C, The expression patterns of the claudins and occludin in the FAE are similar between PP and the cecal patches. Yellow *arrowheads* indicate examples of claudin-4–positive epithelial cells. D, Costaining of PP dome epithelium (FAE) with claudin-4– and ZO-1–specific antibodies. ZO-1 is expressed only in the apical side of the PP epithelia (left column). Claudin-4 is expressed in the apical side as linear signal and is found vaguely in the basolateral side of the epithelial cell (center column). Red (Cy-3) represents ZO-1, green (FITC) represents claudin-4, and the merged picture is also shown (right column).

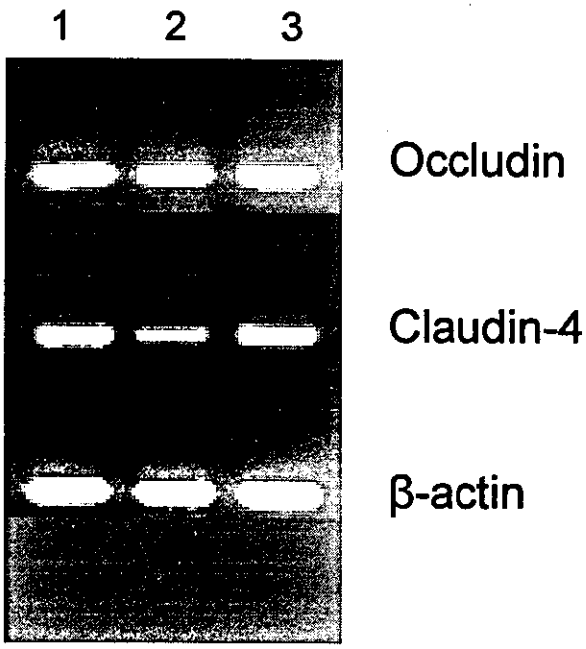

Figure 3.
Semiquantative RT-PCR for the expression of occludin- and claudin-4–specific mRNA by PP and villous epithelial cells. Epithelial cells were isolated from tip and crypt regions of jejunum and FAE of PP by means of a mechanical isolation manner followed by MACS cell sorting. Total RNA was isolated from FAE (*lane 1*), crypt side of villi (*lane 2*), and tip side of villi (*lane 3*). The cDNA amount used for each PCR was equalized by control gene (β-actin). The amplification fragments were visualized on 1.8% agarose gel using ethidium bromide. The levels of occludin-specific mRNA expression are similar among different three samples; however, the level of claudin-4 expression is stronger in FAE of PP and in the villous tip when compared with the villous crypt.

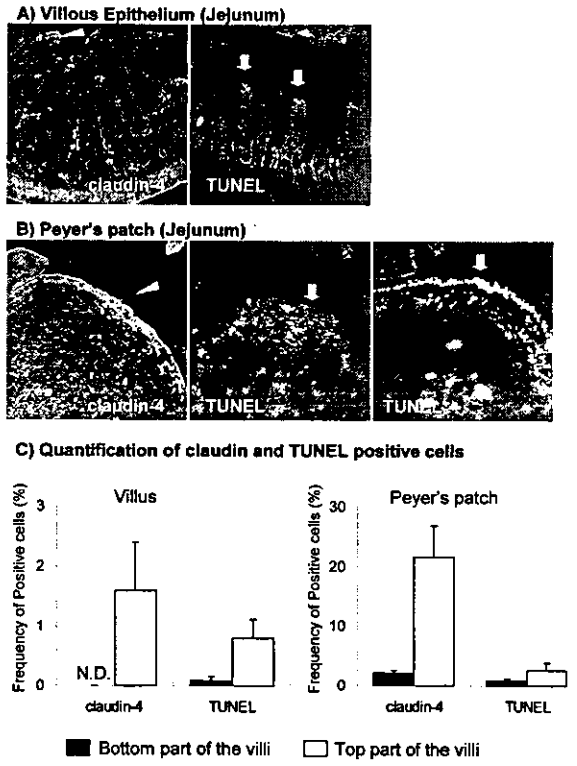

Figure 4.
Relationship of claudin-4 expression and TUNEL (terminal deoxynucleotidyl transferase-mediated dUTP nick-end labeling) staining. TUNEL staining of jejunal villi and the FAE of PP. A, In the jejunum, a few TUNEL-positive cells (*red arrows*) are occasionally present in villous tips, where claudin-4 expression also is present. B, Claudin-4 expression in the FAE of PP is present in the top area of the domes, corresponding to the presence of TUNEL-positive cells. C, Frequency of claudin-4–positive cells and TUNEL-positive cells per villus or per FAE of PP. These FAE has high frequency of both claudin-4– and TUNEL-positive cells; in particular, claudin-4 is expressed preferentially in the top area on the FAE of PP. Data are shown as mean value ± SEM.

apoptotic cells and claudin-4–positive cells was performed (Fig. 4C). In the top part of the villous epithelium, the frequency of claudin-4–positive cells was 1.6 ± 0.8%, whereas in the bottom part of the villi, claudin-4–positive cells were not found. On the other hand, the frequency of TUNEL-positive epithelial cells was 0.8 ± 0.32% in the upper villi and 0.1 ± 0.06% in the lower villi. In terms of the FAE of PP, however, the frequency of claudin-4–positive cells was 2.1 ± 0.6% in the bottom half and 21.6 ± 5.2% in the top half of the FAE. The frequency of TUNEL-positive cells was 0.9 ± 0.3% and 2.6 ± 1.2% in the bottom and top half of the FAE, respectively. Thus, it was shown that FAE of PP had high frequency of both claudin-4– and TUNEL–positive cells; in particular, claudin-4 was expressed preferentially in the top area of the FAE of PP.

PP-Null and Wild-Type Mice Had Similar Patterns of Claudins and Occludin Expression

Next we asked whether the intestines of PP-null mice and wild-type mice have similar or different expressions of claudin and occludin in the intestinal epithelium. We prepared three different kinds of PP-null mice: lymphotoxin α-deficient ($LT\alpha^{-/-}$), cytokine common γ chain-deficient ($C\gamma^{-/Y}$), and NIK-deficient (aly/aly) mice. We found no obvious difference in the distribution of the tight-junction components in either the small intestine (Fig. 5) or large intestine (data not shown) between the various PP-null mice and wild-type mice. We looked especially carefully for a minor difference in claudin and occludin expression in the proximal jejunum and distal ileum of the PP-null mice because PP are most prevalent at these sites in normal mice, but we found no difference.

Discussion

In this study, we examined the distribution of claudin-2, -3, -4, and occludin in murine intestine and the GALT including PP and cecal patches. The results of our various experiments are summarized in Table 1. The major and potentially important finding was the preferential expression of claudin-4 in the dome area of the GALT FAE. In contrast, the expression pattern of other claudins and occludin was similar to that of villous epithelia. In contrast to its sparse expression in the apices of intestinal villi, claudin-4 was prominently expressed in the FAE. Previous studies have shown possible heterogeneity of claudin expression among different locations of tissue or cell type (Furuse et al, 1998; Kiuchi-Saishin et al, 2002; Morita et al, 1999b,

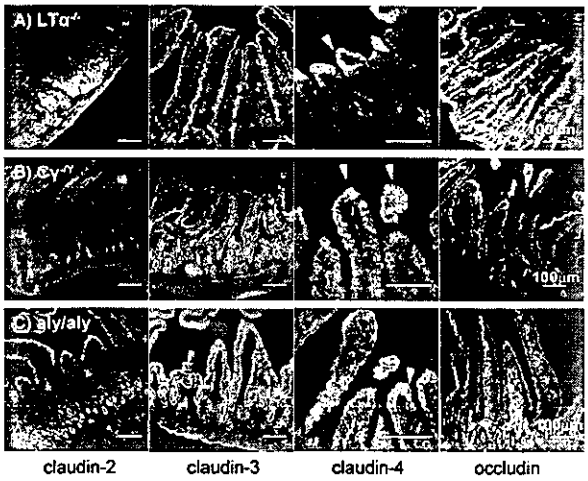

Figure 5.

Claudin expression in villous epithelium of PP-null mice. Immunohistochemical staining of claudin-2, -3, -4, and occludin in the small intestine of PP-null mice. Three different kinds of PP-null mice were examined: lymphotoxin α deficient ($LT\alpha^{-/-}$) (A), common γ chain deficient ($C\gamma^{-/Y}$) (B), and NIK deficient (aly/aly) (C). All of the specimens were prepared from cryosections of jejunum. There is no significant difference in the expression pattern of claudins and occludin in the PP-null mice and wild-type mice: claudin-2 is present in the crypts, claudin-3 and occludin throughout the glands, and claudin-4 only occasionally in villous tips. In the large intestine also, the expression of the claudins and occludin was similar in the PP-null and wild type mice (data not shown). Yellow *arrowheads* indicate examples of claudin-4–positive epithelial cells.

1999c), including a unique distribution in the rat gastrointestinal tract (Rahner et al, 2001). Those studies, though, did not analyze the distribution of claudin and occludin in GALT. The previous study reported that claudin-2 was expressed in the crypts of small and large intestinal epithelia, whereas claudin-3 was found in both crypts and tip regions of intestinal epithelia. Further, claudin-4 was expressed on the tip of villous epithelia of small and large intestines (Rahner et al, 2001). In murine intestinal epithelium, we found claudin-2 expressed in crypts, whereas claudin-3 was expressed in villi and crypts. And claudin-4 was expressed in the villous tips just occasionally, not in every tip. Thus, our data in murine intestines generally agree with the results obtained by the analyses of rat intestinal epithelia, except for the frequency of expression of claudin-4.

The similarity in location of claudin-4 in the epithelium overlying the tips of intestinal villi and the FAE of GALT suggests that claudin-4 has a role in the formation and maintenance of the dome or apex shape of the villi and FAE. Villous epithelial cells are generated in the crypts and proceed upward to the villous tips, and FAE cells similarly are generated in crypts and migrate up to the top of domes of PP and cecal patches, ie, in the hemispherical area. Thus, it seems possible that claudin-4 contributes to maintenance of the hemispherical configuration.

Another possibility is that the expression of claudin-4 is related to the phenomenon of apoptosis because we found a close association between the locations of claudin-4 and apoptotic cells in intestinal villi and the FAE of PP and cecal patches. Also, we noted a correlation between the numbers of TUNEL-positive cells and the expression of claudin-4; claudin-4 was abundant in the FAE of cecal patches, where TUNEL-positive cells were numerous, but was sparse in the villous tips, where apoptotic cells are rare (Hall et al, 1994). We suggest that claudin-4 is involved in the process of peeling off epithelial sheets of apoptotic enterocytes. None of the previous studies examined a potential relationship between claudin expression and cell life cycle, including apoptosis. Another interesting observation in the present study was that claudin-2 in the jejunum and colorectum was associated with the cells located in the epithelial crypts, in contrast to the location of claudin-4 on the apices of villi and the FAE. Taken together, these findings suggest that intestinal epithelial cells may be able to alter their junctional molecules in accordance with their different life cycle stages.

Evidence from this study suggests that claudin-4 expression actually may be associated with loosening of intercellular junctions. The apices of intestinal villi and the FAE are sites where foreign material may enter or be sampled by the gut. For example, some pathogenic microorganisms can invade through the epithelial cells in intestinal villi via intraepithelial dendritic cells (Rescigno et al, 2001; Vazquez-Torres et al, 1999). Since the FAE of GALT, with its associated M cells, is an important antigen-sampling site for the initiation of immune responses (Owen, 1977; Owen et al, 1991), looseness of its intercellular junctions may favor the capturing of antigens. An interesting possibility is that claudin-4 expression contributes to the formation of relatively loose intercellular junctions.

A subset of thymus-derived T cells, ie, CD8$\alpha\beta$ T cells, residing in PP can migrate to intestinal epithelia and become part of the intraepithelial lymphocyte (IEL) pool (Cepek et al, 1994; Shaw et al, 1998). The IELs and their neighboring epithelial cells reciprocally regulate their development and growth via cytokines and corresponding receptor signaling (Fujihashi et al, 1996; Inagaki-Ohara et al, 1997; Yamamoto et al, 1998). Hence, we considered the possibility that some subsets of IEL derived from PP help the regulation of claudin and occludin expression in the intestinal epithelium. However, we found that claudin expression in the villous epithelium of PP-null mice was no different from that of wild-type mice, nor did preprogrammed sites for the development of PP have abnormalities in claudin or occludin expression. These findings suggest that PP-derived IELs are not involved in the regulation of claudin and occludin expression. Currently, we are attempting to determine whether thymus-independent gut-originated T cells have such a function.

Materials and Methods

Animals

C57BL/6 mice and lymphotoxin α-deficient mice ($LT\alpha^{-/-}$) were purchased from Japan CLEA (Tokyo, Japan). NIK-deficient mice (aly/aly) were purchased

Table 1. Summary for the Expression Pattern of Claudin-2, -3, -4, and Occludin in Murine Intestinal Epithelial and FAE of GALT

Animal	Tissue	Claudin-2	Claudin-3	Claudin-4	Occludin
C57BL/6	Jejunum	+ (crypt)	++	± (tip)	++
	Colorectum	+ (crypt)	++	± (tip)	++
	PP (FAE)	−/±	+	++ (tip)	+
	Cecal patch (FAE)	−/±	+	++ (tip)	+
$LT\alpha^{-/-}$	Jejunum	+ (crypt)	++	± (tip)	++
$C\gamma^{-/\gamma}$	Jejunum	+ (crypt)	++	± (tip)	++
aly/aly	Jejunum	+ (crypt)	++	± (tip)	++

−, no expression; ±, occasionally or weakly expressed; +, always expressed; ++, always and strongly expressed.

from SLC (Tokyo, Japan). Cytokine common γ chain-deficient mice ($C\gamma^{-/Y}$) were kindly provided by Dr. H. Ishikawa, Keio University, and were maintained in the Experimental Animal Facility at the Research Institute for Microbial Diseases, Osaka University (Osaka, Japan).

Preparation of Specimens

Mice were killed with 150 mg/kg body weight of ketamine. The whole gastrointestinal tract was then dissected and extensively washed with cold PBS, followed by immersion in Tissue-Tek OCT Compound (SAKURA Finetechnical Company, Ltd., Tokyo, Japan). The specimens were rapidly frozen in liquid nitrogen for cryosectioning. Cryosections were prepared on a Leica Cryostat CM3050S (Leica Microsystems, Wetzlar, Germany) at −20° C in 6 μm thickness. Sections were mounted on glass slides with APS coating (Matsunami Glass Ind., Ltd., Osaka, Japan) and postfixed in 95% ethanol at 4° C for 30 minutes followed by 1-minute acetone fixation. The slides were washed in PBS at 4° C for 10 minutes in preparation for staining.

Antibodies

Rabbit polyclonal anti-mouse claudin-2, -3, -4, and antibodies were raised as described (Furuse et al, 1998). These antibodies specific for the cytoplasmic domains of claudins and occludin were affinity purified on nitrocellulose membranes with glutathione-S-transferase fusion proteins of respective claudin proteins (Furuse et al, 1999; Morita et al, 1999a). Affinity-purified rabbit mAb against occludin (Zymed Laboratories, South San Francisco, California) was used for the detection of occludin expression. Rat mAb against ZO-1 (Chemicon, Temecula, California) was used for double immunohistochemical staining with other tight junctional antibodies.

Isolation of Villous Epithelial Cells and FAE of PP

Single-cell suspensions of epithelial cells were prepared by a mechanical and enzymatic dissociation method using type IV collagenase (Sigma, St. Louis, Missouri) as described previously (Fujihashi et al, 1996; Kawabata et al, 1997; Takahashi et al, 1997). Briefly, after removal of PP, the intestine was opened longitudinally, washed thoroughly, and cut into small fragments. Tip side epithelial cells and IEL were removed from intestinal tissue by incubating in RPMI 1640 (Sigma) containing 2% fetal bovine serum, shaking vigorously, and filtering. After several repetitions of this procedure, the specimens were then minced and added to Joklik's modified medium containing collagenase. Crypt side epithelial cells and lamina propria lymphocytes were dissociated by stirring at 37° C. Then epithelial cells in respective specimens were isolated using the discontinuous density gradient procedure with Percoll (Amersham Pharmacia Biotech, Uppsala, Sweden). Furthermore CD3ε-positive or CD19-positive or MHC class II-positive cells were eliminated by magnetic cell sorting (autoMACS; Miltenyi Biotec, Bergisch Gladbach, Germany). Similar procedures were also performed for the FAE of PP.

RT-PCR for Claudin-4– and Occludin-Specific mRNA

Total mRNA was isolated from MACS-sorted epithelial cells by using TRIzol reagent (Invitrogen, Carlsbad, California), treated with DNase I (Invitrogen), and reverse transcribed into cDNA using PCR buffer (Invitrogen), RNase inhibitor (Toyobo, Tokyo, Japan), $oligo(dT)_{16}$ (Invitrogen), Superscript II reverse transcriptase (Invitrogen), and dNTPs (Amersham Biosciences, Uppsala, Sweden) (Yamamoto et al, 1998). The mixture was incubated at 42° C for 120 minutes and then heated to 90° C for 5 minutes. After treatment with RNase H (Toyobo), the synthesized cDNA and a series of diluted standard oligonucleotides were quantified with a spectrofluorometer using an Oli-Green ssDNA Quantification Kit (Molecular Probes, Eugene, Oregon). PCR amplification from 10 ng of cDNA for each sample was performed with the GeneAmp PCR System 9700 (Perkin-Elmer, Branchburg, New Jersey). RT-PCR was performed using primer pairs for occludin (forward, 5'-ATTATGGTGCCCGTGTCC-3'; reverse, 5'- GAGTAGGGCTTGTCGTTGCT-3') and claudin-4 (forward, 5'- TGGATGAACTGCGTGGTG-3'; reverse, 5'-GGTTGTAGAAGTCGCGGA TG-3') for 35 cycles (94° C, 45 seconds; 52° C, 1 minute; 72° C, 1 minute). These oligonucleotides were synthesized by Asahi Techno Glass (Chiba, Japan). β-actin PCR products were amplified by use of β-actin-specific primer

(forward, 5'-TAGATGGGCACA- GTGTGGG-3'; reverse, 5'-GGCGTGATGGTGGGCA- TGG-3'). The amplified products were separated by electrophoresis on 1.8% agarose gel and visualized with ethidium bromide.

Fluorescence Microscopy

Specimens stained with immunofluorescence reagents were examined and recorded under a fluorescence confocal laser scanning microscope (Micro Radiance MR/AG-2; Bio-Rad, Hercules, California), attached to an Olympus BX50 (Olympus Optical Company, Ltd., Tokyo, Japan).

Immunohistochemical Analyses

Immunohistochemical staining for different claudins and occludin was performed as previously described (Furuse et al, 1999; Morita et al, 1999a), with minor modification. Fixed cryosections were blocked in PBS containing 1% BSA (Sigma) for 30 minutes at room temperature. The sections were incubated with primary antibodies diluted approximately 1:1000 in the blocking buffer for 30 minutes at room temperature and then rinsed twice for 5 minutes each in PBS. The sections were further incubated for 30 minutes at room temperature with secondary antibodies: FITC-conjugated goat anti-rabbit IgG (Chemicon) or Cy-3-conjugated goat anti-rabbit IgG (Jackson ImmunoResearch Laboratories, West Grove, Pennsylvania). Sections were washed three times with PBS and mounted with Immunon Perma Fluor Aqueous Mountant (Thermo Shandon, Pittsburgh, Pennsylvania). As controls, sections were incubated with primary antibody or secondary antibody only. Specimens were observed using a fluorescence confocal microscopy.

TUNEL Staining

Apoptosis in the tissue section was detected by means of the TUNEL method, using ApopTag Fluorescein in Situ Apoptosis Detection Kit (Intergen, Purchase, NY) for fluorescent staining. Cryosections (6 μm) were applied, and the following procedures were performed per protocol. Briefly, postfix was performed with a mixture of 67% volume of ethanol and 33% volume of acetic acid at -20° C for 15 minutes. After washing with cold PBS, the specimens were incubated with terminal deoxynucleotidyl transferase to label the DNA strand breaks for 1 hour at 37° C. Finally, the specimens were reacted with anti-digoxigenin antibody conjugated with FITC for 30 minutes at room temperature in the dark, followed by observation using fluorescence microscopy.

Scoring of Apoptosis and Claudin-4 Cells

Scoring the frequency of TUNEL-positive and claudin-4–positive cells was performed using confocal microscopy as previously described, with minor modification (Marshman et al, 2001). Longitudinal sections of crypts and villi were selected for scoring on the basis that, from the crypt to the tip, they were all in the same section and the crypt lumen was visible. Starting at the base of the crypt column, the cells were examined and counted on both sides and the cells positive for apoptotic fragments (TUNEL) or claudin-4 positive cells were enumerated. For the elucidation of apoptotic cells and claudin-4–expressing cells in murine intestine, the enterocytes in the top one third (tip region) and bottom one third (crypt region) of 20 villi per animal were scored. For the PP, the frequency of apoptotic cells and claudin-4–positive cells was examined in the dome epithelium (or FAE). Selected sections of villi and PP were scored independently for a second time. Comparisons of the numbers of apoptotic and claudin-4-positive cells were analyzed using Student's t test. A p value < 0.05 was considered statistically significant.

References

Anderson JM and Van Itallie CM (1995). Tight junctions and the molecular basis for regulation of paracellular permeability. Am J Physiol 269:G467–G475.

Atisook K and Madara JL (1991). An oligopeptide permeates intestinal tight junctions at glucose-elicited dilatations: Implications for oligopeptide absorption. Gastroenterology 100: 719–724.

Cepek KL, Shaw SK, Parker CM, Russell GJ, Morrow JS, Rimm DL, and Brenner MB (1994). Adhesion between epithelial cells and T lymphocytes mediated by E-cadherin and the alpha E beta 7 integrin. Nature 372:190–193.

Creamer B (1967). The turnover of the epithelium of the small intestine. Br Med Bull 23:226–230.

Fujihashi K, Kawabata S, Hiroi T, Yamamoto M, McGhee JR, Nishikawa S, and Kiyono H (1996). Interleukin 2 (IL-2) and interleukin 7 (IL-7) reciprocally induce IL-7 and IL-2 receptors on gamma delta T-cell receptor-positive intraepithelial lymphocytes. Proc Natl Acad Sci USA 93:3613–3618.

Fujita K, Katahira J, Horiguchi Y, Sonoda N, Furuse M, and Tsukita S (2000). *Clostridium perfringens* enterotoxin binds to the second extracellular loop of claudin-3, a tight junction integral membrane protein. FEBS Lett 476:258–261.

Furuse M, Fujita K, Hiiragi T, Fujimoto K, and Tsukita S (1998). Claudin-1 and -2: Novel integral membrane proteins localizing at tight junctions with no sequence similarity to occludin. J Cell Biol 141:1539–1550.

Furuse M, Hirase T, Itoh M, Nagafuchi A, Yonemura S, and Tsukita S (1993). Occludin: A novel integral membrane protein localizing at tight junctions. J Cell Biol 123:1777–1788.

Furuse M, Sasaki H, and Tsukita S (1999). Manner of interaction of heterogeneous claudin species within and between tight junction strands. J Cell Biol 147:891–903.

Hall PA, Coates PJ, Ansari B, and Hopwood D (1994). Regulation of cell number in the mammalian gastrointestinal tract: The importance of apoptosis. J Cell Sci 107:3569–3577.

Inagaki-Ohara K, Nishimura H, Mitani A, and Yoshikai Y (1997). Interleukin-15 preferentially promotes the growth of intestinal intraepithelial lymphocytes bearing gamma delta T cell receptor in mice. Eur J Immunol 27:2885–2891.

Kawabata S, Boyaka PN, Coste M, Fujihashi K, Hamada S, McGhee JR, and Kiyono H (1997). A novel alkaline

phosphatase-based isolation method allows characterization of intraepithelial lymphocytes from villi tip and crypt regions of murine small intestine. Biochem Biophys Res Commun 241:797–802.

Kiuchi-Saishin Y, Gotoh S, Furuse M, Takasuga A, Tano Y, and Tsukita S (2002). Differential expression patterns of claudins, tight junction membrane proteins, in mouse nephron segments. J Am Soc Nephrol 13:875–886.

Kohbata S, Yokoyama H, and Yabuuchi E (1986). Cytopathogenic effect of *Salmonella typhi* GIFU 10007 on M cells of murine ileal Peyer's patches in ligated ileal loops: An ultrastructural study. Microbiol Immunol 30:1225–1237.

Kops SK, Lowe DK, Bement WM, and West AB (1996). Migration of *Salmonella typhi* through intestinal epithelial monolayers: An in vitro study. Microbiol Immunol 40:799–811.

Marshman E, Ottewell PD, Potten CS, and Watson AJ (2001). Caspase activation during spontaneous and radiation-induced apoptosis in the murine intestine. J Pathol 195:285–292.

McGhee J and Kiyono H (1999), The mucosal immune system, 4th ed. In: Paul WE, editor. Fundamental immunology. Philadelphia: Lippincott-Raven Publishers, 909–945.

Morita K, Furuse M, Fujimoto K, and Tsukita S (1999a). Claudin multigene family encoding four-transmembrane domain protein components of tight junction strands. Proc Natl Acad Sci USA 96:511–516.

Morita K, Sasaki H, Fujimoto K, Furuse M, and Tsukita S (1999b). Claudin-11/OSP-based tight junctions of myelin sheaths in brain and Sertoli cells in testis. J Cell Biol 145:579–588.

Morita K, Sasaki H, Furuse M, and Tsukita S (1999c). Endothelial claudin: Claudin-5/TMVCF constitutes tight junction strands in endothelial cells. J Cell Biol 147:185–194.

Neutra MR, Frey A, and Kraehenbuhl JP (1996). Epithelial M cells: Gateways for mucosal infection and immunization. Cell 86:345–348.

Niedergang F, Sirard JC, Blanc CT, and Kraehenbuhl JP (2000). Entry and survival of *Salmonella typhimurium* in dendritic cells and presentation of recombinant antigens do not require macrophage-specific virulence factors. Proc Natl Acad Sci USA 97:14650–14655.

Owen RL (1977). Sequential uptake of horseradish peroxidase by lymphoid follicle epithelium of Peyer's patches in the normal unobstructed mouse intestine: An ultrastructural study. Gastroenterology 72:440–451.

Owen RL, Piazza AJ, and Ermak TH (1991). Ultrastructural and cytoarchitectural features of lymphoreticular organs in the colon and rectum of adult BALB/c mice. Am J Anat 190:10–18.

Rahner C, Mitic LL, and Anderson JM (2001). Heterogeneity in expression and subcellular localization of claudins 2, 3, 4, and 5 in the rat liver, pancreas, and gut. Gastroenterology 120:411–422.

Rescigno M, Urbano M, Valzasina B, Francolini M, Rotta G, Bonasio R, Granucci F, Kraehenbuhl JP, and Ricciardi-Castagnoli P (2001). Dendritic cells express tight junction proteins and penetrate gut epithelial monolayers to sample bacteria. Nat Immunol 2:361–367.

Savidge TC, Smith MW, James PS, and Aldred P (1991). Salmonella-induced M-cell formation in germ-free mouse Peyer's patch tissue. Am J Pathol 139:177–184.

Schneeberger EE and Lynch RD (1992). Structure, function, and regulation of cellular tight junctions. Am J Physiol 262: L647–L661.

Shaw SK, Hermanowski-Vosatka A, Shibahara T, McCormick BA, Parkos CA, Carlson SL, Ebert EC, Brenner MB, and Madara JL (1998). Migration of intestinal intraepithelial lymphocytes into a polarized epithelial monolayer. Am J Physiol 275:G584–G591.

Sonoda N, Furuse M, Sasaki H, Yonemura S, Katahira J, Horiguchi Y, and Tsukita S (1999). *Clostridium perfringens* enterotoxin fragment removes specific claudins from tight junction strands: Evidence for direct involvement of claudins in tight junction barrier. J Cell Biol 147:195–204.

Takahashi I, Kiyono H, and Hamada S (1997). $CD4^+$ T-cell population mediates development of inflammatory bowel disease in T-cell receptor alpha chain-deficient mice. Gastroenterology 112:1876–1886.

Tsukita S, Furuse M, and Itoh M (2001). Multifunctional strands in tight junctions. Nat Rev Mol Cell Biol 2:285–293.

Vazquez-Torres A, Jones-Carson J, Baumler AJ, Falkow S, Valdivia R, Brown W, Le M, Berggren R, Parks WT, and Fang FC (1999). Extraintestinal dissemination of Salmonella by CD18-expressing phagocytes. Nature 401:804–808.

Yamamoto M, Fujihashi K, Kawabata K, McGhee JR, and Kiyono H (1998). A mucosal intranet: Intestinal epithelial cells down-regulate intraepithelial, but not peripheral, T lymphocytes. J Immunol 160:2188–2196.

Available online at www.sciencedirect.com
SCIENCE DIRECT®
Biochemical and Biophysical Research Communications 315 (2004) 356–362
BBRC
www.elsevier.com/locate/ybbrc

Roles of a conserved family of adaptor proteins, Lnk, SH2-B, and APS, for mast cell development, growth, and functions: *APS*-deficiency causes augmented degranulation and reduced actin assembly

Chiyomi Kubo-Akashi, Masanori Iseki, Sang-Mo Kwon, Hitoshi Takizawa, Kiyoshi Takatsu,* and Satoshi Takaki*

Division of Immunology, Department of Microbiology and Immunology, The Institute of Medical Science, The University of Tokyo, Shirokanedai 4-6-1, Minato-ku, Tokyo 108-8639, Japan

Received 18 December 2003

Abstract

Lnk, SH2-B, and APS form a conserved adaptor protein family. All of those proteins are expressed in mast cells and their possible functions in signaling through c-Kit or FcεRI have been speculated. To investigate roles of Lnk, SH2-B or APS in mast cells, we established IL-3-dependent mast cells from *lnk*$^{-/-}$, *SH2-B*$^{-/-}$, and *APS*$^{-/-}$ mice. IL-3-dependent growth of those cells was comparable. Proliferation or adhesion mediated by c-Kit as well as degranulation induced by cross-linking FcεRI were normal in the absence of Lnk or SH2-B. In contrast, *APS*-deficient mast cells showed augmented degranulation after cross-linking FcεRI compared to wild-type cells, while c-Kit-mediated proliferation and adhesion were kept unaffected. *APS*-deficient mast cells showed reduced actin assembly at steady state, although their various intracellular responses induced by cross-linking FcεRI were indistinguishable compared to wild-type cells. Our results suggest potential roles of APS in controlling actin cytoskeleton and magnitude of degranulation in mast cells.

Keywords: Actin cytoskeleton; Adaptor protein; BMMC; c-Kit; Cytokine; Cytokine receptor; Degranulation; FcεRI; IgE; Signal transduction; Tyrosine kinase

Mast cells play critical roles in allergic and inflammatory responses. Mast cells express the high affinity IgE receptor FcεRI and cross-linking of IgE bound to FcεRI by antigens initiates a series of molecular events in mast cells, which lead to degranulation and release of a wide variety of chemical mediators such as histamine, arachidonic acid metabolites, and soluble proteins including neutral proteases and cytokines [1–3]. Even in the absence of antigen, binding of monomeric IgE to FcεRI induces cytokine production and cell survival [4]. Mast cells differentiate from hematopoietic progenitor cells. Stem cell factor (SCF), which is also known as mast cell growth factor, and IL-3 provide signals for their differentiation, proliferation, and survival mediated through c-Kit receptor tyrosine kinase and IL-3 receptor, respectively. SCF also regulates chemotaxis and adhesion of mature mast cells [1,5].

Lnk, SH2-B, and APS form a conserved family of adaptor proteins, whose members share a homologous N-terminal region with proline rich stretches, PH and SH2 domains, and a conserved C-terminal tyrosine phosphorylation site [6–9]. Lnk plays a critical role in regulating production of B cell precursors and hematopoietic progenitor cells, and functions as a negative regulator of c-Kit-mediated signaling. We have shown that *lnk*$^{-/-}$ mice show enhanced B cell production because of the hypersensitivity of B cell precursors to SCF [8]. In addition, *lnk*$^{-/-}$ mice exhibit increased numbers of hematopoietic progenitors in the bone marrow, and the ability of hematopoietic progenitors to repopulate

* Corresponding authors. Fax: +81-3-5449-5407.
E-mail addresses: takatsuk@ims.u-tokyo.ac.jp (K. Takatsu), takakis@ims.u-tokyo.ac.jp (S. Takaki).

0006-291X/$ - see front matter © 2004 Elsevier Inc. All rights reserved.
doi:10.1016/j.bbrc.2004.01.060

irradiated host animals was greatly enhanced by the absence of Lnk [10]. Independently, Velazquez et al. [11] have reported *lnk*-deficiency results in abnormal modulation of SCF and IL-3-mediated signaling pathways and augmented growth of bone marrow cells or splenocytes. SH2-B is originally identified as a protein associated with immunoreceptor tyrosine-based activation motifs (ITAMs) of FcεRI γ-chain by a modified two-hybrid (tribrid system) screening [6]. We have shown that SH2-B is a critical molecule for the maturation of reproduction organs that is at least in part mediated by insulin-like growth factor I (IGF-I) receptor signaling [12]. APS is identified as a potential substrate of c-Kit by two-hybrid system [7]. We also independently isolated the murine counterpart of APS as a protein homologous to Lnk and SH2-B [9]. APS is phosphorylated upon stimulation with various growth factors, including EPO-R, PDGF-R, insulin, nerve growth factor (NGF), and cross-linking B cell receptor (BCR) [9,13–16]. Recently, we generated $APS^{-/-}$ mice and found that B-1 cells in peritoneal cavity were increased, and humoral immune responses to type-2 antigen significantly enhanced in $APS^{-/-}$ mice [17].

Lnk-family adaptor proteins, Lnk, SH2-B, and APS, are all expressed in bone marrow-derived mast cells (BMMCs) [12]. In addition, various experiments using cell lines overexpressing those Lnk-family adaptor proteins suggested their possible functions in signaling mediated through c-Kit or FcεRI. We investigated and compared for the first time consequences of the deficiency either of Lnk, SH2-B or APS in mast cell functions using primary cultured cells. We established BMMCs from bone marrow progenitors of $lnk^{-/-}$, $SH2\text{-}B^{-/-}$, $APS^{-/-}$ mice, and their respective control wild-type mice. IL-3-dependent BMMCs were equally established even in the absence of Lnk, SH2-B or APS. SCF-dependent proliferation or adhesion was also not compromised and was comparable among $lnk^{-/-}$, $SH2\text{-}B^{-/-}$, and $APS^{-/-}$ BMMCs. Although FcεRI-mediated degranulation was not affected by the absence of Lnk or SH2-B, $APS^{-/-}$ BMMCs showed enhanced degranulation after cross-linking FcεRI. $APS^{-/-}$ BMMCs showed reduced filamentous actin (F-actin) assembly at steady state and was resistant to inhibitors disrupting F-actin microfilaments in FcεRI-mediated degranulation responses. These results suggest that APS plays a role in negative regulation of mast cell degranulation by controlling actin dynamics.

Materials and methods

Cells and culture. Bone marrow cells were obtained from 8- to 10-week-old $lnk^{-/-}$ [8], $SH2\text{-}B^{-/-}$ [12], $APS^{-/-}$ mice [17], and their respective wild-type littermates, and cultured in RPMI1640 supplemented with 5 ng/ml murine IL-3 (PeproTech), 8% fetal calf serum (FCS), nonessential amino acids (Gibco-BRL), 100 IU/ml penicillin, 100 μg/ml streptomycin, and 10 μM of 2-mercaptoethanol. Cells were split and supplied with fresh medium every 4 or 5 days. After 4 weeks of cultivation, greater than 95% of cells were c-Kit and FcεRI positive as assessed by flow cytometry.

Flow cytometry and cytochemistry. For the detection of FcεRI, BMMCs were incubated in a supernatant of IGEL a2 (15.3) hybridoma containing mouse anti-DNP IgE monoclonal antibody (mAb) and then stained with fluorescein isothiocyanate (FITC)-conjugated anti-mouse IgE mAb (LO-ME-2, Oxford Biomarketing, UK). For the detection of c-Kit, cells were stained with phycoerythrin (PE)-conjugated anti-CD117 mAb (2B8, Pharmingen). For measurements of F-actin content, cells were fixed in 3.7% formaldehyde for 6 h at 4 °C permeabilized with 0.2% Triton X-100 in PBS for 30 min and then stained with rhodamine-conjugated phalloidin (Molecular Probes, Eugene, OR) for 1 h. Stained cells were then analyzed by flow cytometry using a FACSCalibur (Becton–Dickinson).

Unstimulated or stimulated BMMCs were resuspended in PBS and deposited onto microscope slides using a Cytospin 3 (Shandon Scientific, Cheshire, England). After staining with May–Gruenwald's and Giemsa's solutions (MERCK), cellular morphology was assessed by a light microscope.

Proliferation and survival assays. BMMCs (5×10^4) were cultured in 0.2 ml of flesh medium containing various concentrations of SCF (PeproTech) in a 96-well multi-well plate for 72 h. Cells were pulsed with [^{3}H]thymidine (0.2 μCi/well) in the last 12 h of culture and harvested and incorporated [^{3}H]thymidine was measured in triplicate determination using a MATRIX 96 Direct Beta Counter (Packard, Meriden, CT). Cells were cultured in media alone or in the presence of various concentrations of anti-DNP IgE mAb (SPE-7, Sigma). Percentage of viable cells was determined by trypan blue exclusion.

Adhesion assay. Adhesion assays to fibronectin were performed as previously described [18]. In brief, 5×10^4 BMMCs labeled with 2′,7′-bis-(2-carboxyethyl)-5-(and-6)-carboxy fluorescein (BCECF: Molecular Probes, Eugene, OR) were incubated in triplicate in a 96-well polystyrene plate (Lynbro-Titertek, Aurora, OH) coated with fibronectin (Sigma) in the presence of various concentrations of SCF or 10 ng/ml PMA at 37 °C for 30 min. Unbound cells were removed by washing the plates with binding medium RPMI 1640 containing 10 mM Hepes (pH 7.4), and 0.03% BSA four times. Adhered cells were quantified by measuring fluorescence of input and bound cells using a Fluorescence Concentration Analyzer (IDEXX Laboratories, Westbrook, ME).

Degranulation assay. BMMCs were sensitized with anti-DNP IgE at 37 °C for 18 h, washed, and resuspended in Tyrode's buffer (10 mM Hepes, pH 7.4, 130 mM NaCl, 5 mM KCl, 1.4 mM $CaCl_2$, 1 mM $MgCl_2$, 5.6 mM glucose, and 0.1% BSA). Cells (5×10^5 in 0.2 ml) were then stimulated with various concentrations of DNP-BSA or 10 ng/ml PMA plus 400 ng/ml ionomycin at 37 °C for 1 h. Enzymatic activities of β-hexosaminidase in supernatants and cells solubilized in 0.5% Triton X-100 Tyrode's buffer were measured using *p*-nitrophenyl *N*-acetyl-β-D-glucosaminidase (Sigma) as substrates. Degranulation was calculated as the percentage of β-hexosaminidase released from cells in the total amount of the enzyme in the supernatants and cell pellets as described before [18]. For the experiment using latrunculin, sensitized BMMCs were pretreated with various concentrations of latrunculin for 15 min at 37 °C before assays. Histamine released into culture supernatants after degranulation was measured using ELISA kit (Immunotech, Marseille, France) according to manufacturer's recommendation.

Calcium measurements. Sensitized BMMCs were incubated with 6 μM Fura PE3/AM (TEFLABS, Austin, TX) in PBS containing 20 mM Hepes (pH 7.4), 5 mM glucose, 0.025% BSA, and 1 mM $CaCl_2$ (HBS) at 37 °C for 60 min. Cells were washed and resuspended in HBS (1×10^5 cells/0.1 ml) in a stirring cuvette. Fluorescence was monitored continuously with a fluorescence spectrophotometer (CAF-110: JASCO, Osaka, Japan) at an emission wavelength of 500 nm and two different excitation wavelengths (340 and 380 nm).

Immunoblotting. Cell lysates from stimulated BMMCs were subjected to immunoprecipitation and Western blot analysis as previously

described [9]. The proteins were resolved by SDS–8% PAGE and transferred to PVDF membranes (Immobilon, Millipore). After blocking with 5% BSA, membranes were probed with anti-phosphotyrosine mAb (4G10, Upstate Biotechnology) and incubated with HRP-conjugated secondary antibodies. Blots were washed in 0.05% Tween 20/Tris-buffered saline, pH 7.6, and proteins were detected by chemiluminescence (Perkin-Elmer Life Sciences).

Results

Establishment of BMMCs lacking either Lnk, SH2-B or APS

Lnk, SH2-B, and APS were all expressed in normal BMMCs [12]. To investigate possible functions of those adaptor proteins in mast cells, we established IL-3-dependent BMMCs from bone marrow progenitors of *lnk*$^{-/-}$, *SH2-B*$^{-/-}$, and *APS*$^{-/-}$ mice and their responses were compared with those of BMMCs established from respective control wild-type littermates. IL-3-dependent growth of *lnk*$^{-/-}$, *SH2-B*$^{-/-}$ or *APS*$^{-/-}$ bone marrow progenitor cells was almost comparable to that of respective control progenitor cells (Fig. 1A). Established *lnk*$^{-/-}$, *SH2-B*$^{-/-}$ or *APS*$^{-/-}$ BMMCs were not distinguishable from the wild-type BMMCs in terms of surface expression of FcεRI and c-Kit (Fig. 1B). Mast cell differentiation and proliferation induced by IL-3 was not affected at all even in the absence of Lnk, SH2-B or APS.

Functions of lnk$^{-/-}$, *SH2-B*$^{-/-}$ *or APS*$^{-/-}$ *BMMCs*

First, we examined proliferative responses of established BMMCs to SCF and found no difference among *lnk*$^{-/-}$, *SH2-B*$^{-/-}$, *APS*$^{-/-}$, and respective control BMMCs (Fig. 2A). Adhesion to fibronectin induced by SCF or PMA was also not affected in the absence of Lnk, SH2-B or APS (Fig. 2B). We then examined degranulation of those BMMCs induced by cross-linking FcεRI by measuring β-hexosaminidase and histamine released after stimulation. Degranulation from *lnk*$^{-/-}$ or *SH2-B*$^{-/-}$ BMMCs was almost comparable to that from control wild-type BMMCs (Fig. 2C). In contrast, *APS*$^{-/-}$ BMMCs showed enhanced degranulation responses upon cross-linking FcεRI (Fig. 2C). Degranulation from *APS*$^{-/-}$ BMMCs, determined by β-hexosaminidase releasability, was 130–140% of that from control cells at each stimulation condition, and the enhancement was statistically significant at the concentrations of DNP-BSA over 0.5 μg/ml (Table 1). Histamine released after cross-linking FcεRI was also augmented in *APS*$^{-/-}$ BMMCs (data not shown).

FcεRI-mediated cellular responses in APS$^{-/-}$ *BMMCs*

To clarify the possible molecular mechanisms leading to the enhanced degranulation in the absence of APS,

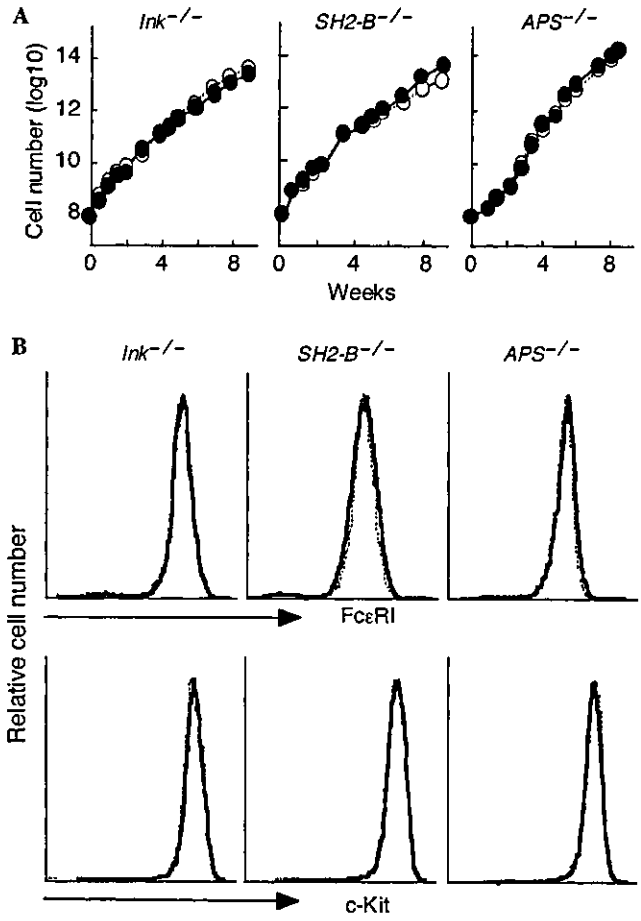

Fig. 1. (A) Cumulative cell numbers of *lnk*$^{-/-}$, *SH2-B*$^{-/-}$, *APS*$^{-/-}$ (closed circles), and respective wild-type control (open circles) BMMCs. Differentiation of BMMCs from progenitors and their cell growth induced by IL-3 was comparable in the absence of either Lnk, SH2-B or APS. Representative results obtained from multiple independent pairs of BMMCs are shown. (B) Surface expressions of FcεRI (upper panels) or c-Kit (lower panels) on *lnk*$^{-/-}$, *SH2-B*$^{-/-}$, *APS*$^{-/-}$ (bold lines), and respective wild-type control (dotted lines) BMMCs. After IgE sensitization, BMMCs were stained with anti-c-Kit or anti-IgE antibodies and analyzed by flow cytometry. Representative results of multiple independent experiments are shown.

we tried to evaluate various cellular events induced by cross-linking FcεRI. We first cytochemically evaluated the proportion of degranulated BMMCs after stimulation. Percentage of degranulated cells increased in a dose-dependent manner as the concentration of antigens increased. Importantly, the ratio of degranulated BMMCs in each stimulation condition was comparable between *APS*$^{-/-}$ and wild-type BMMCs (Fig. 3A). The enhanced degranulation from *APS*$^{-/-}$ BMMCs was thus due to augmented degranulation from each mast cell but not to increased proportion of cells that underwent degranulation. We then analyzed calcium influx induced by cross-linking FcεRI, however, we did not observe significant difference in initial peak and following sustained increase of intracellular free calcium between *APS*$^{-/-}$ and control BMMCs (Fig. 3B). Cell survival

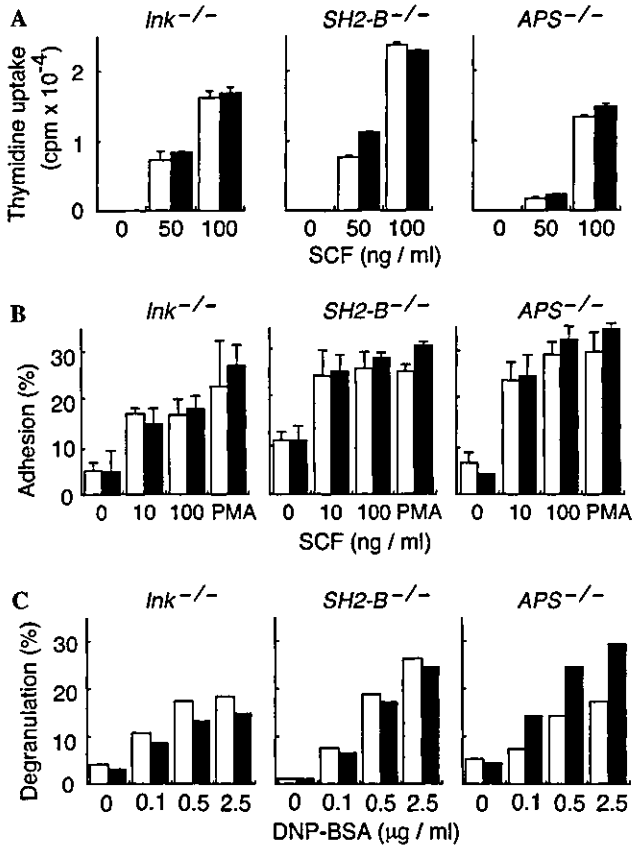

Fig. 2. Responses of $lnk^{-/-}$, $SH2\text{-}B^{-/-}$ or $APS^{-/-}$ BMMCs (filled bars) and of respective control BMMCs (open bars) induced by activation of c-Kit or FcεRI. (A) Proliferation upon stimulation with various concentrations of SCF. Values shown are the mean cpm ± SD of triplicate determinations. (B) Adhesion to fibronectin induced by various concentrations of SCF or 10 ng/ml PMA. Shown are average ± SD of triplicate measurements. (C) Degranulation after cross-linking FcεRI. Cells sensitized with anti-DNP IgE mAb were stimulated with the various concentrations of DNP-BSA. Shown is the percentage of β-hexosaminidase activity released into culture supernatants out of the total β-hexosaminidase initially stored in cells. $APS^{-/-}$ BMMCs showed augmented degranulation responses (see also Table 1). Representative results of three independent experiments are shown from (A) through (C).

mediated by binding of monomeric IgE to FcεRI was also comparable (Fig. 3C). Tyrosine phosphorylation of various cellular proteins was rapidly induced after cross-linking FcεRI in mast cells and was comparable between $APS^{-/-}$ and wild-type BMMCs. Phosphorylation of neither Akt nor PKCδ molecules was affected in the absence of APS (data not shown).

Decreased actin assembly in $APS^{-/-}$ BMMCs

It has been shown that Lnk associates with an actin binding protein ABP-280 [19] and that SH2-B plays a role in actin reorganization and cell motility mediated by growth hormone receptor [20,21]. We recently found that Lnk facilitates actin reorganization in transfected fibroblast cells (S.M.K. and S.T., unpublished data). In addition, a negative correlation between actin polymerization and FcεRI-mediated degranulation from RBL-2H3 mast cell line has been presented [22,23].

We speculated APS may regulate actin cytoskeleton, which potentially has regulatory process for degranulation in mast cells. Therefore, we investigated consequences of inhibition of actin polymerization induced by cross-linking FcεRI in BMMCs and its effect on degranulation by treatment with latrunculin. Treatment of sensitized BMMCs with latrunculin resulted in the reduction of F-actin contents as demonstrated by rhodamine–phalloidine binding (Fig. 4A, left panel). Cross-linking FcεRI induced reduction of F-actin contents in stimulated BMMCs. Consistent with observations using RBL-2H3 cells, inhibition of actin assembly by treatment with latrunculin enhanced degranulation from normal BMMCs in a dose-dependent manner (Fig. 4A, right). Interestingly, sensitized $APS^{-/-}$ BMMCs showed reduced F-actin content (about 70% of control) compared to wild-type cells (Fig. 4B, left). The reduction in F-actin contents became less evident in cells treated with latrunculin. Finally, the effect of latrunculin on degranulation was compared between $APS^{-/-}$ and control BMMCs. As shown in Fig. 4B, augmented degranulation by $APS^{-/-}$ BMMCs became less evident by treatment with latrunculin, which was well correlated with difference in F-actin contents between latrunculin treated $APS^{-/-}$ and control cells. These results suggested that *APS*-deficiency in mast cells made actin assembly at relatively low levels and that resulted in facilitated degranulation process after cross-linking FcεRI.

Table 1
Enhancement of FcεRI-induced degranulation in $APS^{-/-}$ BMMC

DNP-BSA(μg/ml)	Degranulation (% maximal response induced by PMA plus ionomycin)			
	0	0.1	0.5	2.5
+/+ ($n = 11$)	5.6 ± 0.9	19.4 ± 2.4	28.9 ± 2.5	29.4 ± 2.1
−/− ($n = 11$)	5.0 ± 0.7	25.8 ± 3.9	39.5 ± 3.9*	40.6 ± 3.4**
(% +/+ response)	(89%)	(133%)	(136%)	(138%)

Sensitized BMMCs were stimulated with the various concentrations of DNP-BSA or 10 ng/ml PMA plus 400 ng/ml ionomycin. Values represent the mean ± SE of % β-hexosaminidase activity normalized by the value induced with PMA plus ionomycin as 100%. *$p < 0.05$, **$p < 0.01$ compared to +/+ BMMCs by Student's t test.